Tornadogenesis in High-end Tornadic Supercells (Part 2)
The Descending Reflectivity Core, Inflow Channel and Streamwise Vorticity Current

Chris Broyles[1], Corey Potvin[2], Greg Dial[1], James Murnan[2], Steven Shores[4], Andrew Lyons[1], Matthew Elliott[1], Ashton Robinson Cook[3]

[1] NOAA/NWS/NCEP/Storm Prediction Center, Norman, Oklahoma
[2] NOAA/National Severe Storms Laboratory, Norman, Oklahoma
[3] Weather Prediction Center, [4] University of Oklahoma Student

Abstract

A database of 208 supercells that produced tornadoes rated EF3 to EF5, was created at the Storm Prediction Center to collect data on observed features involved in high-end tornadogenesis. WSR-88D high-resolution radar was used to identify the descending reflectivity core (DRC) and inflow channel associated with supercells in the database. Evidence was gathered for the streamwise vorticity current (SVC). Using the 208 case average, the tornado formed as the leading edge of the DRC hit the center of the RFD occlusion. For 20 representative cases, the DRC approached the RFD occlusion from the west-southwest at around 50 knots. For 18 cases within a quarter mile of the RFD occlusion, the maximum wind speed within the DRC was estimated by radar to be over 80 knots. The DRC reached the ground southwest of the RFD occlusion with the tornado forming on the northern side of the DRC. The study provided evidence for the following hypothesis. 1) The DRC appears to be critical to tornado formation because a sharp increase in wind speeds translates through the DRC. When this area of high winds reaches the RFD occlusion, rotational velocity in the surface mesocyclone rapidly strengthens. 2) The DRC provides a sheltering effect for a column of vertical vorticity that organizes on the DRC's lee side that appears to protect the developing tornado from strong vertical shear, keeping the circulation from being torn apart.

An inflow channel was found on reflectivity for 193 of the 208 supercells (92.8%). For the 208 case average, the inflow channel began about five minutes prior to the tornado start time and ended about 16 minutes after the tornado start time, with a duration of around 21 minutes. During the analysis of these events, evidence was gathered to hypothesize that the SVC forms in response to the developing inflow channel. The likely zone for horizontal vorticity generation is along the supercell's forward flank precipitation gradient, within the northern part of the inflow channel. This is where the inflow-outflow interface is present, and upward motion runs parallel to downward motion. As the inflow channel is created, wind speeds inside it were estimated to generally double. This is theorized to be due to the Bernoulli Effect, which creates a pressure drop within the inflow channel and across the northeast quadrant of the RFD. This pressure drop deepens a surface low within the RFD, which strengthens the RFD occlusion. The inflow channel is associated with strong vertical motion, which creates the southern side of the SVC. Environmental flow that does not enter into the inflow channel must go up and over the top. When it reaches the forward flank downdraft, the air dives toward the surface and is drawn back into the inflow channel. This completes the horizontal circulation within the SVC. Evidence and reasoning for this hypothesis are presented using several case studies and observations.

1. INTRODUCTION

Much work has been done over the last seven decades concerning tornadogenesis in supercells. In the latter half of the 20th century, many studies have focused on the role of the descending reflectivity core (DRC) in tornado formation. Some of these studies include Magsig et al. 2002, Rasmussen et al. 2006, Kennedy et al. 2007, Byko et al. 2009, French et al. 2015, and Houser et al. 2018 Other studies on tornadogenesis include Klemp and Rotunno 1983, Davies-Jones et al. 2001, Davies-Jones 2006, Markowski and Richardson 2009, and Kosiba 2013. Additional work has shown evidence of an inflow channel and streamwise vorticity current (SVC) in model simulations. After the turn of the century, a new focus was made on the SVC with high resolution modeling. In the last few years, new conceptual advances have been made concerning the supercell inflow region and SVC. Some papers on these features include Klemp and Rotunno 1983, Dowell and Bluestein 1997, Shabbott and Markowski 2004, Kosiba et al. 2013, Beck and Weiss 2013, French et al. 2015, Orf et al. 2017, 2018, Schueth 2018, Dixon 2019, Peters et al. 2019, 2020, Nowotarski 2020 and Schueth et al. 2021.

This project aims to further expand on the work that has been done to advance our understanding of the DRC, inflow channel and SVC. The focus was to learn more about tornadogenesis and how the various supercell features contribute to the formation of high-end tornadoes.

2. METHODOLOGY

In order to put together the puzzle pieces of high-end tornadogenesis, we determined that a relatively large sample of supercells with high-end tornadoes would be needed. High-resolution radar would be analyzed for measuring as many characteristics of these supercells as possible. An archive of WSR-88D high-resolution radar, at the Storm Prediction Center, would be used to satisfy most requirements for data collection. Other data, including surface observations and soundings, would be used to collect environmental information. It was determined that about a decade of radar data would be needed for this project. The period in the archive from May 22, 2008 to December 31, 2019 was examined. Before a case was added to the spreadsheet, seven criteria must be met (listed below).

1) A supercell mesocyclone must be present in velocity data. The mesocyclone was identified on the lowest elevation angle using storm relative velocity, unless otherwise stated.
2) A forward flank must exist, distinguishing it from a bow echo. Forward flanks were evident with storms that had a mesocyclone.
3) The lowest elevation cut through the low-level mesocyclone must be at 8,000 feet or less.
4) An RFD occlusion, associated with tornado development, must not be preceded by another RFD occlusion within the previous 5 minutes.
5) At least one volume scan without an RFD occlusion, must be present between RFD occlusions.
6) A one-minute gap must exist between the tornado being analyzed and the end of the previous tornado.
7) High-resolution radar must be available for storms more than 50 nautical miles from the radar. High-resolution radar was used for 20 of the 26 storms on April 27, 2011. Low-resolution radar was used for six on that day, all within 50 nautical miles of the radar.

After these criteria were applied to each case, a database was established consisting of 208 supercells associated with EF3 to EF5 tornadoes. The dates and times of each tornado were entered onto a spreadsheet using the Storm Events Database. For one case, the tornado start time was adjusted five minutes earlier, based on a debris ball and 91 knot gate-to-gate shear.

3. DESCENDING REFLECTIVITY CORES

During the analysis, it became apparent that a relatively small-scale pronounced reflectivity maxima was almost always associated with the start of a high-end tornado. This finding in our large database is consistent with the smaller database in Kennedy et al. 2006. These reflectivity maxima were almost always a separate entity and moved toward or around the rear flank downdraft (RFD) occlusion just prior to tornado formation.

Byko et al. 2009 used the term "discrete reflectivity maxima" (DRM), to describe such a feature. Other studies have found a reflectivity maximum near developing tornadoes (Magsig et al. 2002, Rasmussen et al. 2006). We found that for high-end tornadic supercells, these DRMs were almost always descending reflectivity cores (DRCs). As was discussed in part 1, these DRCs commonly appeared to be instigated by the first cell merger documented for each tornadic supercell in this database. For the 208 cases, this cell merger occurred on average about 15 minutes prior to the tornado start time, with the DRC forming shortly thereafter. Figure 1 shows the temporal distribution of the start time of cell merger one (blue), the DRC (red) and the RFD Surge (green). Within 7 minutes of the tornado start time, the distributions are clustered close together. From about 13 to 30 minutes prior to the tornado, DRC initiation occurred just after cell merger one, with the RFD surge beginning about two minutes after cell merger one.

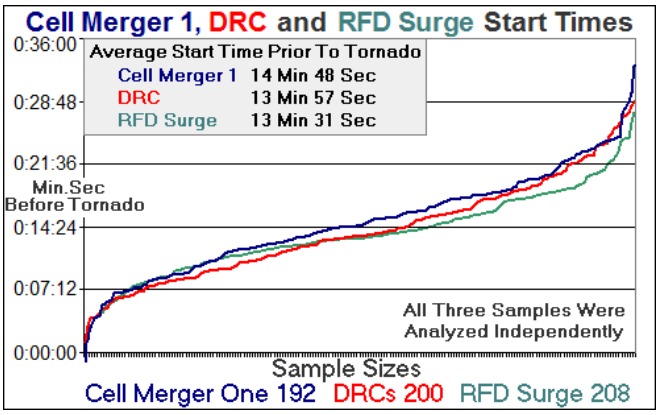

Figure 1. The sorted start time distributions of the first cell merger (blue), the DRC (red) and RFD surge (green) associated with tornadogenesis for each supercell. There appears to be a relationship between the three. On average, cell merger one occurred just before DRC initiation and over a minute before the start of the RFD surge. All three were analyzed independently.

On average, the DRC forms and moves toward the RFD occlusion from the west-southwest, decreasing in diameter over time. The leading edge of these DRCs often reached the RFD occlusion near the tornado start time. The DRCs were often associated with a wind speed max sloped at various angles, depending upon environmental factors. The DRCs could be characterized as an internal RFD surge, well documented in the Bowdle, South Dakota tornadic storm on May 22, 2010 (Lee et al. 2012).

These descending reflectivity cores appeared to be critically important to tornadogenesis and were consistently present during the process. A goal of this study has been to find commonality among all cases in tornadogenesis so that potential causation can be determined. Because of that, we do not use a low-end threshold to eliminate low reflectivity DRCs. We found that some Great Plains cases had DRCs with reflectivity maxima that were consistently below 50 DBZ. Examination for these cases suggested that the role of these DRCs was similar to their higher reflectivity counterparts, and that these DRCs likely played an important role in tornadogenesis. For these cases, the highest wind speeds within the higher reflectivity DRCs were similar to the highest wind speeds within the lower reflectivity DRCs.

We found that the DRC would either descend behind the flanking line precipitation or within it. Sometimes, the DRC would remain partially attached to the flanking line precipitation. These partially attached DRCs were evident in manual analysis and appeared to play a similar role in tornadogenesis compared to DRCs that remained discrete. Because of this, we devised a qualification system that would capture both discrete DRCs and attached DRCs. For this reason, we found a higher percentage of storms with DRCs than has been found in other studies. Using a wider DRC definition enabled this study to document the commonality between all the tornadic supercells in the database.

For a DRC to be identified and analyzed by the system, the descending reflectivity core must be apparent in reflectivity data. The DRC must descend on a cross-section for at least 3 scans, with at least two of three meeting the criteria below. 86% of the time, the DRC drop sequence was over 3 scans.

1) The bin with the highest reflectivity value within the DRC must be at least 5 DBZ greater than 80 percent of the reflectivity bins just outside of the edge of the DRC. The DRC for any one scan could fall under one of three categories for enclosure, including 100 percent, 95 to 99.9 percent and 80 to 94.9 percent.
2) The area of enhanced reflectivity must drop at a nearly constant angle of descent, except toward the end when an increased rate of drop was allowed. It was found that the average rate of descent increased by 51 percent as the DRC approached the ground.
3) The area of enhanced reflectivity must be located near or within the supercell's pendant or developing hook echo within 5 minutes of the tornado start time.

To begin the analysis technique, reflectivity and base velocity scans using the WSR-88D high-resolution radar, were examined to identify a discrete reflectivity maximum (DRM) in the vicinity of the RFD occlusion just prior to the tornado start time for all 208 supercells. To identify a potential DRC, a similar approach was taken to the cell merger analysis in Part 1. First, a series of reflectivity scans was examined for each supercell prior to the development of the tornado. A discrete reflectivity maximum was identified, making sure there was temporal and spatial continuity. Then, the location of the potential DRC was found on the reflectivity scan nearest to the tornado start time at the lowest elevation angle.

After all DRMs were identified, cross-sections were examined along each DRM's path to determine if it was a descending reflectivity core (DRC) according to the three criteria above. As a result, 200 of the 208 cases (96.2%) were designated as DRCs. The other 8 cases were considered DRMs. For these 8 cases, the elevation of the lowest elevation angle could be above the DRC's path or the DRC could be too small to see using the WSR-88D. The breakdown of DRCs is as follows.

Total DRCs Identified
200 of 208 (96.2%)

DRCs With All Scans Having
100 Percent Enclosure Within The Drop Sequence
84 of 208 (40.4%)

DRCs With At Least One Scan Having
95 Percent Enclosure As Lowest In The Drop Sequence
41 of 208 (19.7%)

DRCs With At Least One Scan Having
80 Percent Enclosure As Lowest In The Drop Sequence
69 of 208 (33.2%)

DRCs with One Scan Having
No Maximum Within A Drop Sequence of At Least 3 Scans
6 of 208 (2.9%)

125 of the 208 (60.1%) supercells had a DRC with at least 95 percent enclosure for all scans within the drop sequence. The average DRC drop sequence for all DRCs was 4.6 scans.

Figure 2 shows a collection of 12 DRCs near the tornado start time, with the smallest component of each DRC encircled in white. On each panel, the location of either the tornado (T) or RFD occlusion (O) is marked.

On the cross-sections, the DRCs often appeared to break away from a larger area of precipitation higher up in the supercell. The larger area of precipitation would continue to move horizontally, while the DRC would separate and start a downward trajectory. During the analysis, we had to be careful to draw the cross-section exactly along the path of the DRC. That would eliminate the illusion of a core developing if an already matured core came into the cross-section from the side. This would appear as an increasing area of precipitation,

DRCs In Different Sizes and Shapes (Circled Near Tornado Start Time)

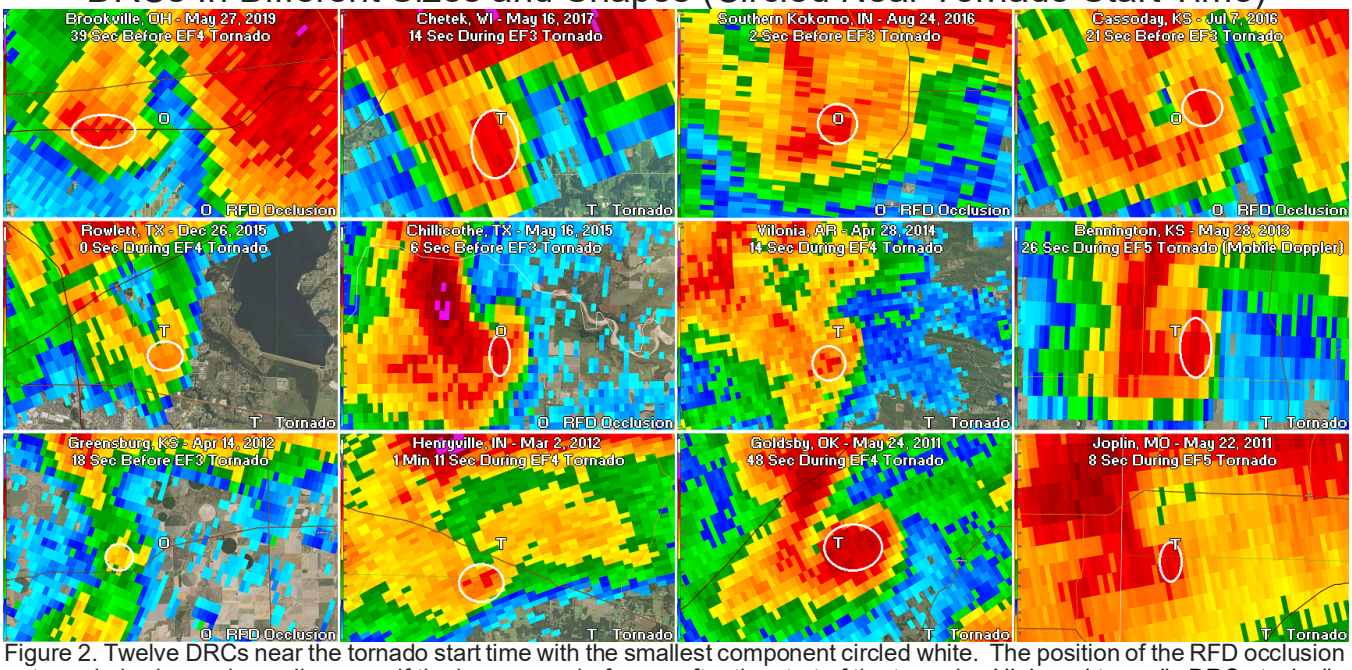

Figure 2. Twelve DRCs near the tornado start time with the smallest component circled white. The position of the RFD occlusion or tornado is shown depending upon if the image was before or after the start of the tornado. High-end tornadic DRCs typically approached the RFD occlusion from the west-southwest and wrapped into the RFD occlusion near the tornado start time.

expanding upward and downward at the same time. Also, some DRC paths were slightly curved, especially after tornado formation, requiring careful cross-section placement to maximize the distance along the DRC path. The DRCs were generally located on the southern edge of the flanking line precipitation, where reflectivity became lighter. The DRCs were either discrete cells south or southwest of the pendant, or cells embedded in the pendant. The DRCs often took on an elongated concave wedge shape during the drop period, with the concavity pointed vertically. The rear of the DRC would hit the ground first. Then, a zipper-like effect would occur with the DRC moving into the ground from the rear to the middle, and then from the middle to the front. The tornado would often form near this time, as the DRC's nose hit the RFD occlusion.

Figure 3 shows the DRC associated with the EF3 tornado for the Chillicothe, Texas supercell on May 16, 2015. As with many cases, this DRC formed just after a cell merger (panel 4 and 5). In panels 6 through 10, the DRC gradually descends to the surface, taking on an elongated concave wedge shape in panel 8. The tornado forms just after the center of the DRC is estimated to have begun impacting the ground (panel 9).

Cell Merger and DRC Drop Sequence for Chillicothe, Texas Supercell on May 16, 2015

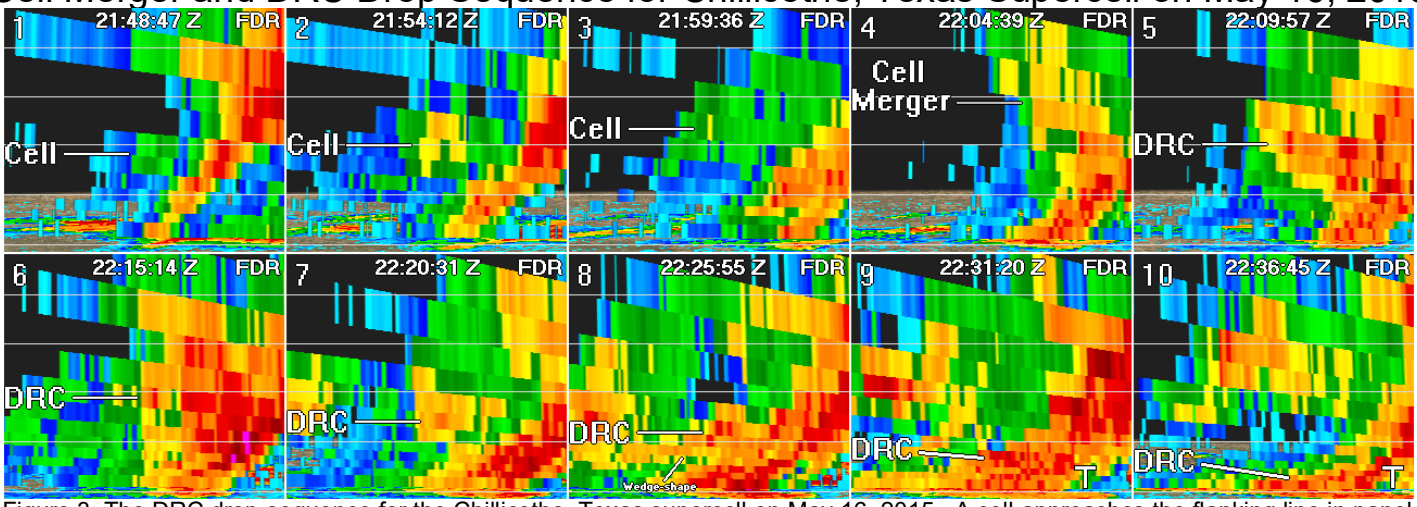

Figure 3. The DRC drop sequence for the Chillicothe, Texas supercell on May 16, 2015. A cell approaches the flanking line in panel 1 to 3, and merges with the flanking line in panel 4. The DRC develops in response to the cell merger and drops toward the surface (panels 5 to 10). The DRC takes on an elongated concave wedge shape in panel 8. The tornado begins in panel 9 just after the center of the DRC is estimated to have begun impacting the ground.

The most recent 63 DRCs were examined in greater detail. This part of the dataset had shorter time between scans, providing more temporal resolution. For these cases, the DRC's start time and elevation were recorded using the first reflectivity scan that the DRC was evident. Then, the number of scans for the entire drop sequence was recorded. After this, an examination was done to estimate the time that the center of the DRC first touched the ground. And fourth, an examination was done to estimate the time that the center of the DRC reached the ground. For these last two time estimates, a systematic approach was developed to interpolate the most likely time of occurrence between scans. To interpolate a time, three divisions were made between scans. For the cross-sections, the average time between scans was around 4 minutes. The three divisions between scans were about a minute apart. The first division was early between scans. The second division was midway between scans. And the third division was late between scans.

To help make the time estimates consistent, reflectivity and base velocity radar signatures were identified for estimating the ground impact time. There were four key signatures identified. The first was an extension signature.

For this signature, a gap must exist between the descending reflectivity max or the associated wind speed max, and the lowest elevation angle. To identify this signature, a narrow connection of higher reflectivity or higher wind speeds had to bridge the gap at the lowest elevation angle. If this signature was found, then a "late between scans" time was designated.

A second DRC signature was found for estimating an impact time half way between scans. This signature involved a closing gap between the descending reflectivity max or DRC's wind speed max, and the lowest elevation angle. To identify this signature, a relatively wide connection must be present at the lowest elevation angle. If this signature was found, then a "midway between scans" time was designated.

A third DRC signature was found, called a "dome signature". This involved a relatively wide and flat upside down U-shape, usually with a pronounced reflectivity max inside at the lowest elevation angle. When this signature was identified, either an "early between scans" or "midway between scans" time was designated, depending upon the DRC's descent rate and on whether the dome signature was stretched out or compact. Once the interpolated times were found, an estimate was made for ground impact time using the height of the lowest elevation angle and the rate of descent of the DRC.

At the left in both Figure 4 and 5, reflectivity cross-sections are shown with the DRCs for the Chetek, Wisconsin EF3 and the New Orleans East, Louisiana EF3. For the Chetek case, the DRC begins attached to the flanking line precipitation, meeting the 80 percent enclosed criteria. For both cases, the DRC begins in panel one and then takes on an elongated concave wedge shape in panel 2 before reaching the lowest elevation angle in panel 3. For both cases, a dome signature is present in panel 3. The New Orleans East case has a wider and more compact dome signature than the Chetek case, suggesting that the New Orleans East DRC has been at the lowest elevation angle for a bit longer than for the Chetek case. For both cases, the DRC is estimated to have begun impacting the lowest elevation angle between panel 2 and 3, with the impact time for New Orleans East designated "early between scans" and for Chetek designated "midway between scans".

At the right in both Figure 4 and 5, base velocity cross-sections are shown associated with the DRCs for the Pawnee Rock, Kansas EF3 and Katie, Oklahoma EF4. In both cases, the stronger winds in the DRC descend from the upper left to the lower right (panel 1 to 3). The Pawnee Rock case has a narrow extension signature in panel 3, suggesting the stronger winds have just begun to impact the lowest elevation angle. For this case, the estimated lowest elevation angle impact time would be "late between scans". The Katie case has a stretched out dome signature in panel 3, which is much wider than the extension signature for the Pawnee case. For the Katie case, the estimated lowest elevation angle impact time would be "midday between scans", which would be a bit earlier than the Pawnee Rock case. For all four cases in Figure 4 and 5, actual ground impact times were calculated using the DRC's estimated descent rate in the lowest 10,000 feet above ground and the height of the lowest elevation angle. In Figure 6, the estimated ground impact time of the DRC's center is shown for 63 EF3 to EF5 supercells.

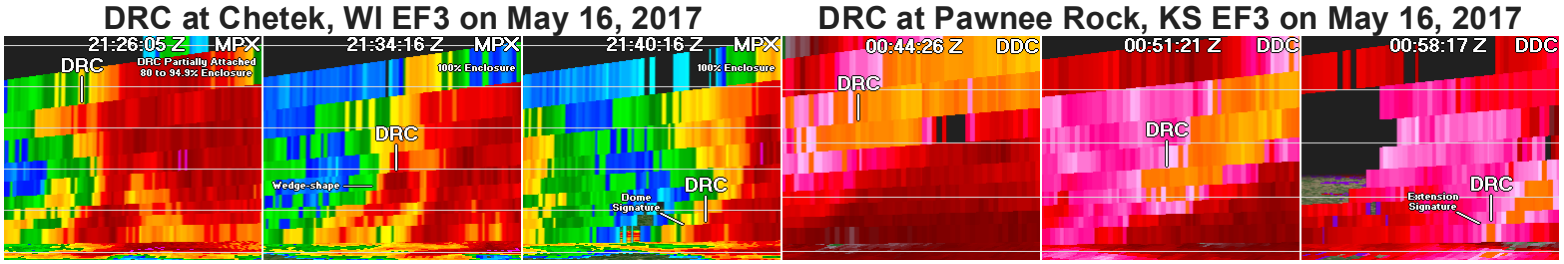

Figure 4. At the left, a reflectivity cross-section for the DRC at Chetek, WI. At the right, a base velocity cross-section for the DRC at Pawnee Rock, KS. In both cases, the DRC descends from upper left to lower right. The Chetek DRC takes on a long concave wedge shape (panel 2).

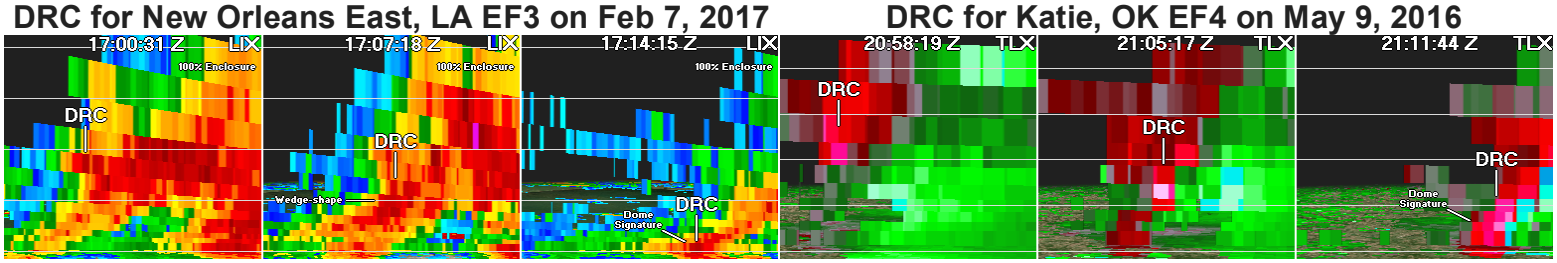

Figure 5. At the left, a reflectivity cross-section for the DRC at New Orleans East, LA. At the right, a base velocity cross-section for the DRC at Katie, OK. In both cases, the DRC descends from upper left to lower right. The New Orleans East DRC takes on a long concave wedge shape (panel 2).

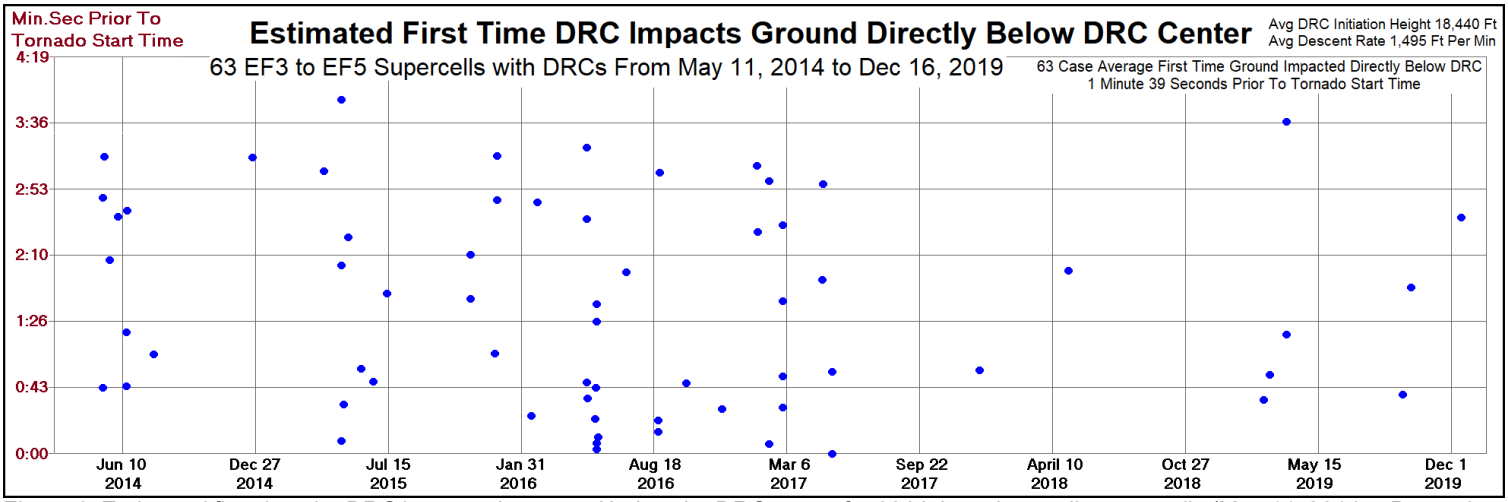

Figure 6. Estimated first time the DRC impacts the ground below the DRC center for 63 high-end tornadic supercells (May 11, 2014 to December 16, 2019). The distribution shows the times relative to the tornado start time. On average, the DRC's center impacted the ground 1 minute 39 seconds before the tornado start time. On average, the DRCs initiated at 18,440 feet AGL and descended at 1,495 feet per minute.

On average, for 18 DRCs within a quarter nautical mile of the radar, analysis showed that the DRC hit the ground to the southwest of the RFD occlusion.

Once the DRC reaches the surface, tornado formation could involve downward momentum transfer and vortex line tilting, followed by vorticity stretching (Byko et al. 2006). But these processes likely happen quickly. Our results show that on average, the tornado often forms as the DRC wraps into the RFD occlusion's ground circulation. Similar to this study's results, a downward pressure gradient was found to wrap around the southeast side of the Arcadia, Oklahoma mesocyclone during tornadogenesis on May 17, 1981 (Hane and Ray 1985, Dowell and Bluestein 1997).

The DRCs for the first 104 cases were analyzed in greater detail and categorized into three types.

In Figure 7, the first type of DRC is for the Shawnee, Oklahoma EF4 tornado on May 19, 2013. For a Type 1 DRC (39 cases), it usually forms 5 to 10 minutes before the tornado starts. For this type, a rapid intensification of the DRC occurs as it approaches the RFD occlusion, with the intensification taking place a few minutes before the tornado.

In Figure 8, the second type of DRC is for the Vilonia, Arkansas EF4 tornado on April 27, 2014. For a Type 2 DRC (28 cases), it usually forms 15 to 20 minutes before the tornado starts. After the DRC forms, a gradual increase in reflectivity or size occurs at the lowest elevation angle (below 3,000 feet) up until tornado formation. Just after the tornado starts, a brief decrease in intensity occurs 71.4% of the time. This happened for the Vilonia case (second panel from right). The average elevation for the 28 cases of Type 2 was 1,424 feet.

In Figure 9, the third type of DRC is for the Rochelle, Illinois EF4 tornado on April 9, 2015. For a Type 3 DRC (26 cases), it usually forms 10 to 15 minutes before the tornado starts. After the DRC forms, a gradual decrease of reflectivity or size occurs at the lowest elevation angle (above 3,000 feet) up until tornado formation.

For the Rochelle case, the radar initially sampled the DRC's center at an elevation of 5,716 feet (first panel at left). By the time the DRC reached the RFD occlusion (middle panel), the radar sampling elevation of the DRC's center had dropped to 5,157 feet. Therefore, the decrease of intensity within the DRC was not due to the beam elevation becoming higher. It could have been related to dry air being ingested into the RFD making the DRC appear to decrease in intensity. The average elevation for the 26 cases of Type 3 was 4,828 feet.

DRC Type 1 (37.50%) - Rapid Intensification Just Before Tornado

EF4 at Shawnee, Oklahoma on May 19, 2013

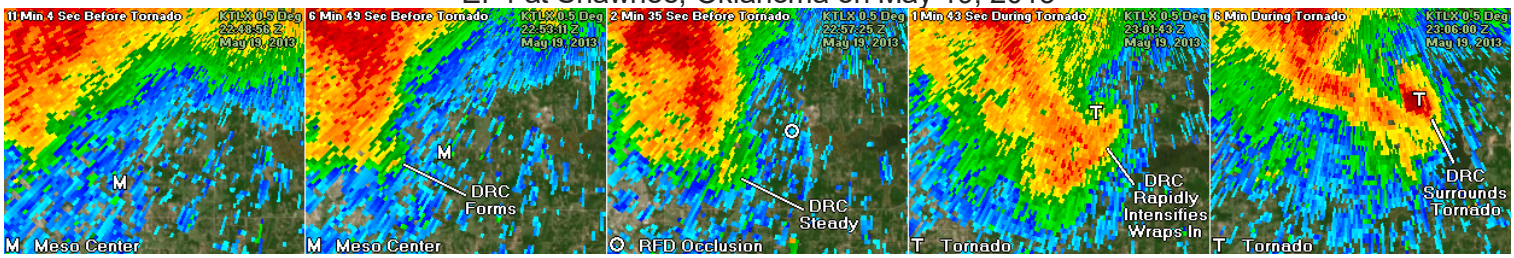

Figure 7. The DRC associated with the EF4 at Shawnee, Oklahoma on May 19, 2013. (DRC Elevation Varies From 550 Feet Left to 289 Feet Right).

DRC Type 2 (26.92%) - Gradual Increase In Intensity Before Tornado (Below 3,000 Feet)

EF4 at Vilonia, Arkansas on April 27, 2014

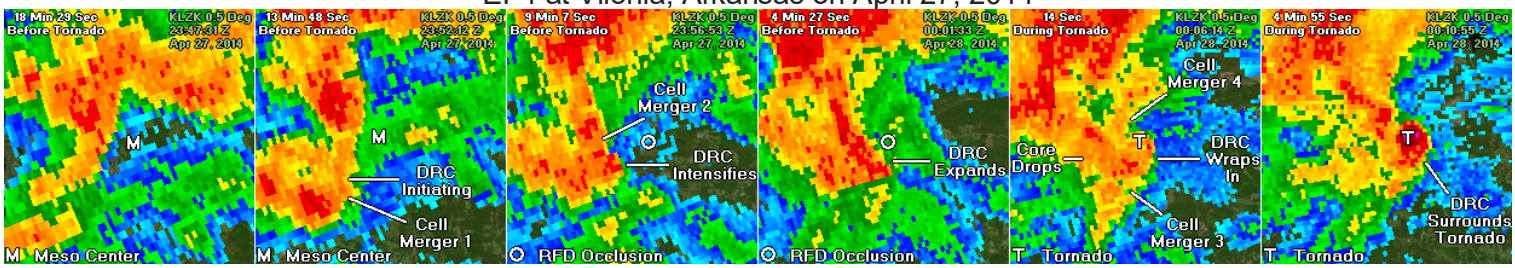

Figure 8. The DRC associated with the EF3 at Vilonia, Arkansas on April 27, 2014. (DRC Elevation Varies From 2,087 Feet Left to 1,138 Feet Right).

DRC Type 3 (25.0%) - Gradual Decrease In Intensity Before Tornado (Above 3,000 Feet)

EF5 at Rochelle, Illinois on April 9, 2015

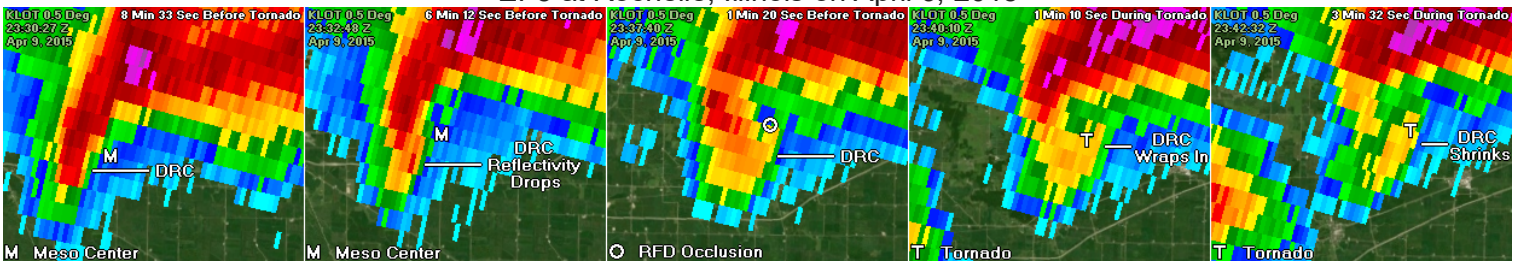

Figure 9. The DRC associated with the EF4 at Rochelle, Illinois on April 9, 2015. (DRC Elevation Varies From 5,716 Feet Left to 4,845 Feet Right).

After a potential DRC was found nearest to the tornado start time for each of the 208 supercells, the location was marked on a transparency relative to the tornado start location. The resulting plots were made in Figure 10 and 11. These plots show the distribution of DRCs relative to the tornado start position. Near the tornado start time, the highest incidence of DRCs was 0.4 nautical miles southwest of the tornado. For the 208 case average, the DRC was instigated by cell merger one. Then, cell merger two contributed to DRC intensification. This process is detailed in Part 1. After the two cell mergers, the DRC would organize and hit the RFD occlusion, likely playing an important role in tornadogenesis.

Descending Reflectivity Core Location Relative To Tornado Start Location (200 DRCs, 8 DRMs)

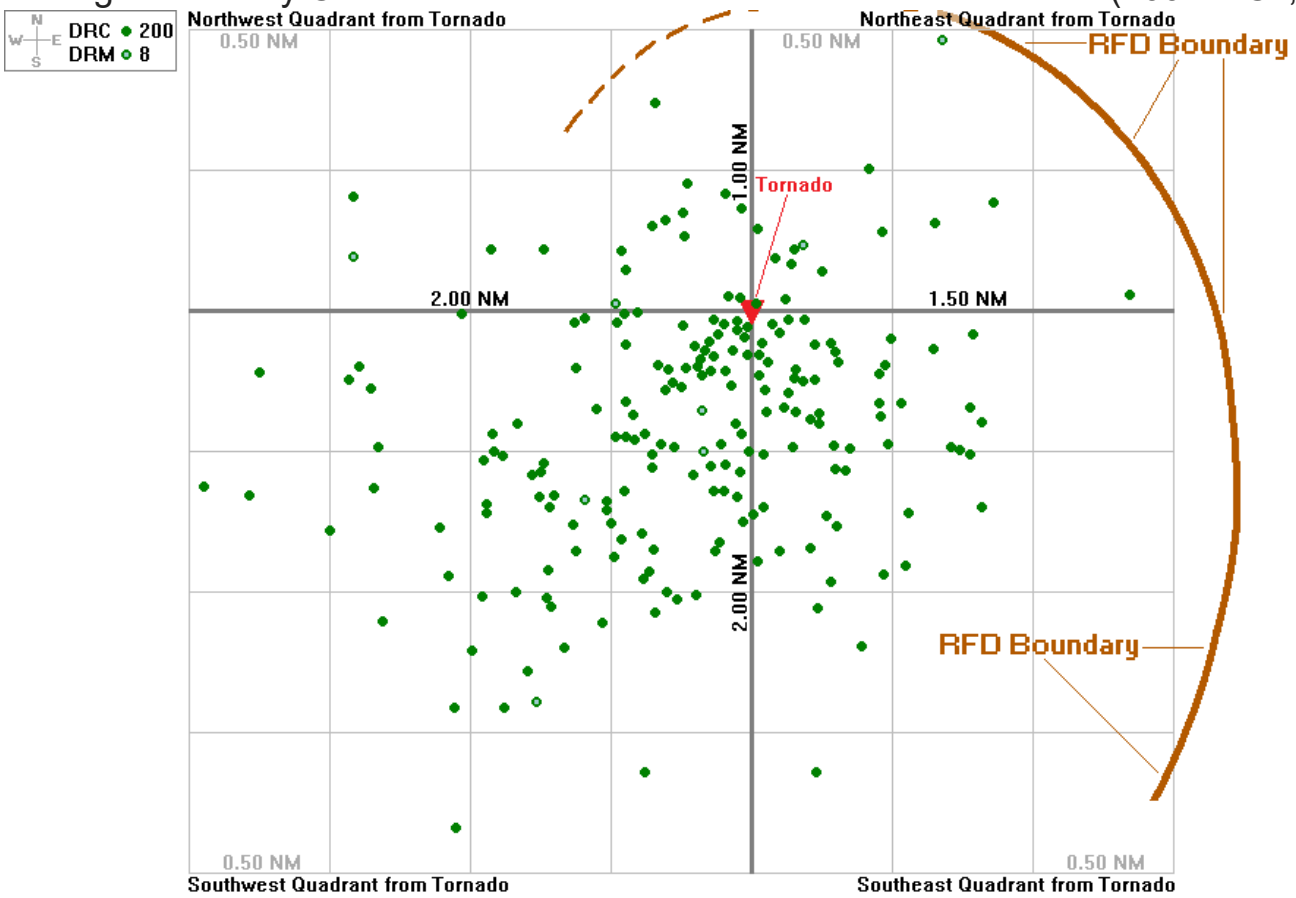

Figure 10. The distribution of 200 DRCs and 8 DRMs relative to the tornado start location. The average RFD boundary location is shown relative to the case distribution.

Descending Reflectivity Core Frequency Relative To Tornado Start Location (200 DRCs, 8 DRMs)

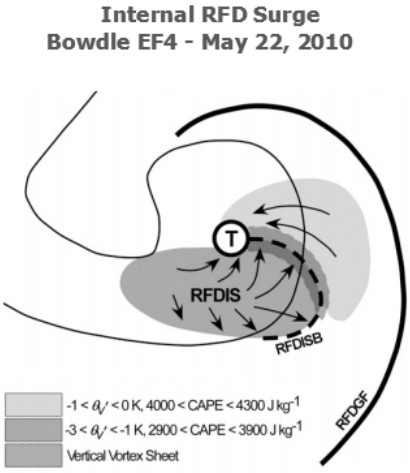

The rear flank downdraft internal surge (RFDIS) associated with rapid intensification phase of the Bowdle, South Dakota EF4 tornado on May 22, 2010 from Lee et al. 2012. The position of the internal surge and RFD boundary (RFDGF) is very similar to the graphic at the right, which shows the 208 case distribution of DRCs, along with the average position of the RFD boundary.

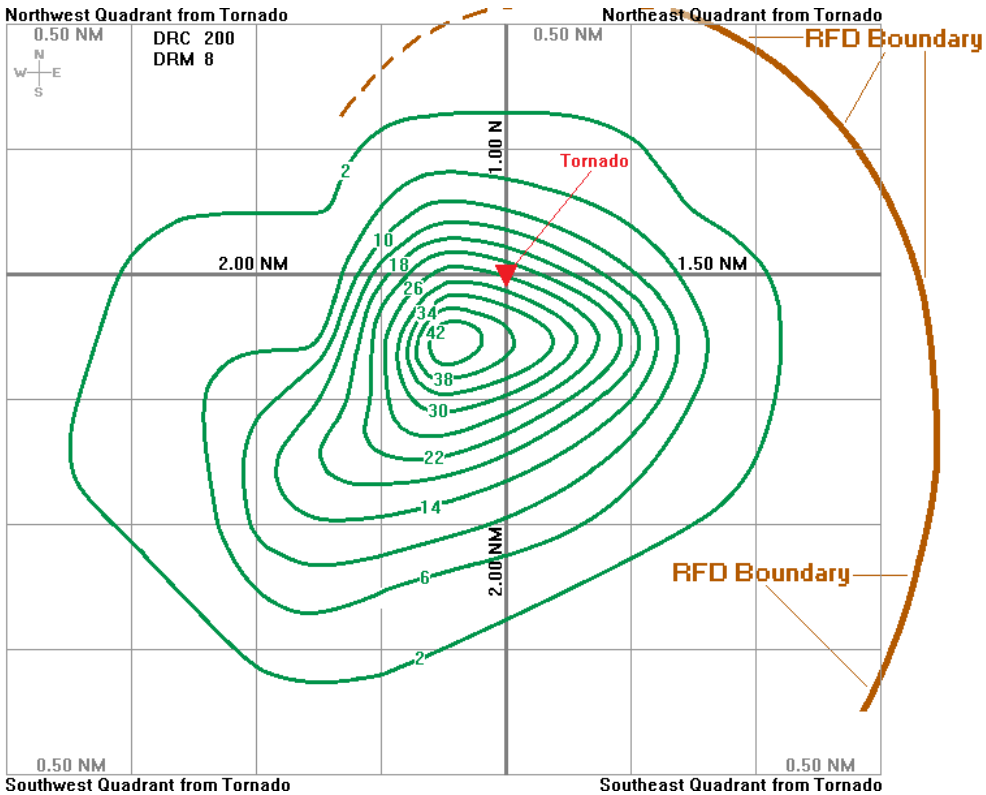

Figure 11. A contoured plot to the right showing the distribution of 200 DRCs and 8 DRMs relative to the tornado start location. The graphic to the left is similar, showing the internal RFD surge (RFDIS) for the Bowdle, South Dakota EF4 just to the south-southwest of the tornado (T), from Lee et al. 2012. The RFDIS is in a similar location to the maximum occurrence of DRCs for the 208 case database. The average RFD boundary positions are also similar in both graphics relative to the maximum in DRC occurrence.

DRC Location Relative To Tornado Start Location (200 DRCs and 8 DRMs)

(Separated Temporally and Spatially)

Cases 1 to 104 (7.75 Years)
March 15, 2012 to December 16, 2019

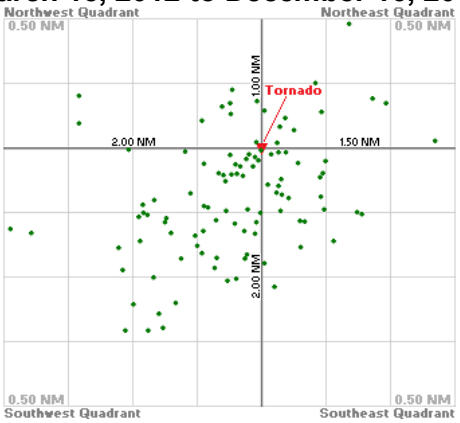

East of Mississippi River

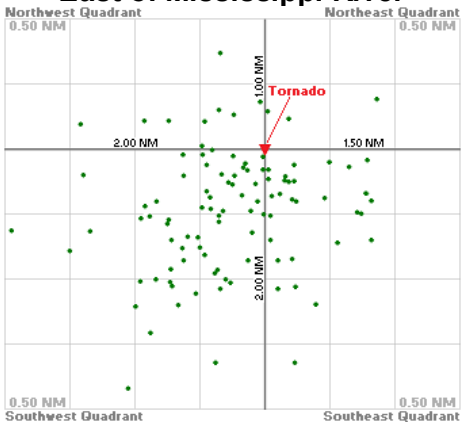

May 22, 2008 to March 2, 2012
Cases 105 to 208 (3.77 Years)

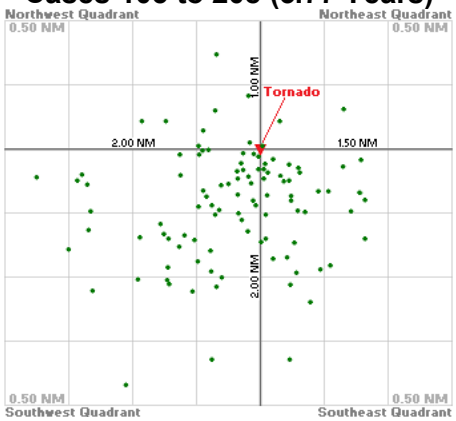

West of Mississippi River

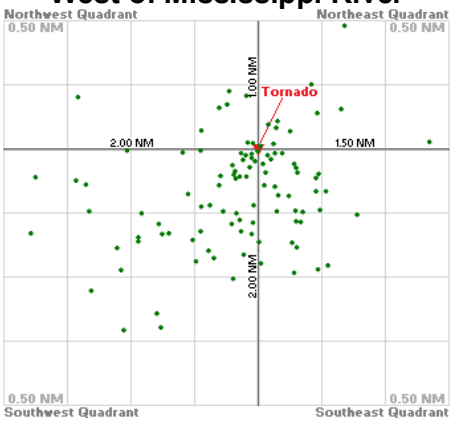

Figure 12. The distribution of 200 DRCs and 8 DRMs divided into four parts. The cases 1 to 104 are shown at the upper left, while the cases 105 to 208 are shown at the lower left. The cases to the east of the Mississippi River are shown at the upper right, while the cases to the west of the Mississippi River are shown at the lower right.

The distribution of 200 DRCs and 8 DRMs was divided into four parts for the graphics in Figure 12. For the two plots at the left, the 208 cases are divided in half. The first 104 cases (March 15, 2012 to December 16, 2019) are plotted in the top left graphic with the second 104 cases (May 22, 2008 to March 2, 2012) in the bottom left graphic. The two distributions are similar with the earlier time period (lower left) being more concentrated to the south of the tornado. This earlier period was dominated by large tornado outbreaks, while the later period (upper left) was not. That means that during the earlier period, the environments surrounding the supercells were more similar in nature. The earlier period includes April 27, 2011, March 2, 2012, May 24, 2011 and April 10, 2009. These outbreaks alone contributed 46 (44.2%) of the tornadic supercell cases on the plot (lower left). The graphics to the right in Figure 12 also have similar distributions. The graphic west of the Mississippi River (lower right) is more concentrated especially just south of the tornado start location.

After the distribution plot was made in Figure 10, the time differences of the reflectivity scan used to identify the DRC and the actual tornado start time were calculated. Once the calculations were made, the resulting scan-to-tornado time difference for each case was plotted on the DRC distribution graphic in Figure 10. The graphic in Figure 13 on the next page, was made by dividing the plot into four sections and then averaging the time differences for all the cases in each section. The result shows how critical the timing of the DRC is to tornado development.

The average times are later and later in each section from west-southwest to east-northeast across the plot. This increase in times toward the east-northeast reflects the movement of the DRC. Analysis shows that the DRC moves toward the RFD occlusion, on average from the west-southwest, then curves toward the north on the eastern side of the circulation.

Analysis for all 208 cases shows that the DRC consists of an area of maximized reflectivity moving toward the RFD occlusion from the west-southwest at an average speed of around 50 knots. As the DRC approaches the RFD occlusion, a relatively small area of very strong winds is generated, averaging just over 80 knots for 18 cases within a quarter mile of the RFD occlusion. The speed max in the DRC was found on base velocity at the lowest elevation angle. An adjustment was made based on the difference of the estimated wind and beam directions (explanation in section 5). These strong winds translate eastward to the nose of the DRC by the time the leading edge of the DRC arrives at the RFD occlusion. Radar projections of the DRC show the strong winds hit the ground just to the southwest of the RFD occlusion. These winds then wrap cyclonically around the circulation's eastern side. For this database, the DRC's leading edge reached the RFD occlusion simultaneously with the start of the tornado.

In a technical sense, for the 208 cases in the database on average, the tornado began nearly coincident with the DRC's leading edge reaching the RFD occlusion (Figure 13). A discussion on the temporal precision of our results is given in the section 8.

Tornado Forms Upon Arrival of the DRCs Leading Edge (208 Case Average)

Difference of DRC Analysis Radar Scan Time To Tornado Start Time, Times Averaged
In Four Areas Relative To Tornado Start Location To Measure Time of DRC Arrival

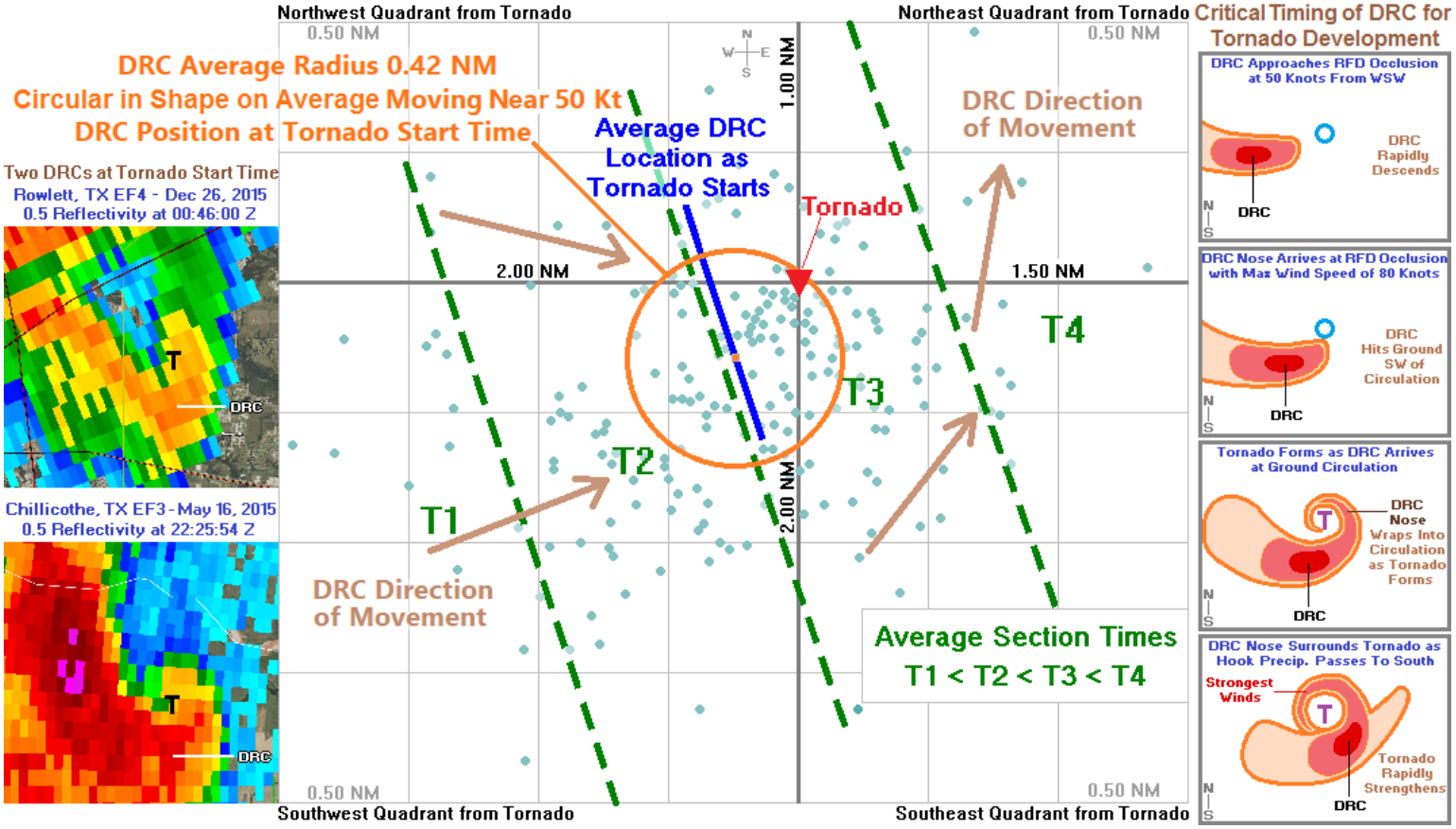

Figure 13. The graphic shows the difference of the reflectivity scan time used to identify the DRC and the tornado start time. Average times are grouped into four sections labeled T1, T2, T3 and T4. The average time for the cases in each section is later and later from left to right. This shows the DRC movement from the west-southwest toward the RFD occlusion. At the tornado start time, the DRC's highest incidence is located approximately 0.38 nautical miles southwest of the tornado start location with the leading edge of the DRC near the tornado start location.

Radar analysis shows that the tornado most often develops just to the north of the DRC, within a tight gradient of reflectivity, on the DRC's lee side. A hypothesis based on this observation was made that the DRC blocks airflow from reaching the RFD occlusion on the south side, forcing a concentrated channel of higher wind speeds to the east and north of the RFD occlusion. An observation of the Bowdle, South Dakota EF4 supercell shows this idea at the left in Figure 11 (Lee et al. 2012). We hypothesize that the Bernoulli Effect (defined in section 5) contributes to wind speed enhancement and reduces pressure within the cavity created by curvature in the DRC. Within this cavity, a protected column of relatively undisturbed air is created, in which vertical vorticity can be more easily organized. This sheltering effect appears to protect the column of vertical vorticity from stronger vertical shear, making it easier for the low-level mesocyclone to stretch vertical vorticity upward and keeping the developing tornado from being torn apart. In Fischer et al. 2022, a similar idea is presented, that a weaker updraft-relative flow is favorable because the developing vortex stays in the updraft region longer and becomes less tilted. In Figure 13, this cavity, mentioned in our hypothesis, can be seen for the two cases at the left and in the series of DRC graphics to the right.

Concerning the DRC's timing for the cases in the database, the 208 case average had the tornado developing immediately after the DRC arrived at the RFD occlusion. The "Average DRC Location at Tornado Time" was marked by using interpolation between the average times in the two middle sections. This line crosses through the location of highest DRC incidence, 0.38 nautical miles southwest of the tornado start location. Then, a test was done to determine the average shape of the DRCs. Although DRCs are generally ovular, the test revealed the average DRC shape as a circle because of the averaging process of various DRC directional orientations.

On average, DRCs were much larger at further distances away from the RFD occlusion. The size of the DRC decreased by 33 percent as it approached the RFD occlusion. The average diameter near the tornado start time for all 208 DRCs was measured to be 0.84 nautical miles (1.56 kilometers). This diameter was used to draw a circle on Figure 13, highlighting the approximate area encompassed by the DRC. This average diameter is larger than the one kilometer diameter of a DRC mentioned in Rasmussen et al. 2006, although some DRCs in the database were around one kilometer in diameter.

In Figure 13, the average edge of the circle (DRC's leading edge) at the tornado start time is very near the tornado start location. After this was discovered, the top 20 EF4-EF5 supercells closest to the 208 storm average were examined. The speed of the DRC for each case was calculated using a series of reflectivity scans at the lowest elevation angle. The speed for the 20 DRCs was near 50 knots. This was 153% faster than the average speed of the 20 supercells.

In Figure 14, a DRC was observed by Brian Barnes of StormTours.com during the development of the Bennington,

Kansas EF3 tornado on May 28, 2013. The video is located at www.youtube.com/watch?v=6VuUnKKyNyw. The video captures look northwest. In the upper first and second panels, the Bennington tornado is just starting. While subtle, the DRC is to the left of the Bennington tornado. This DRC shared visual characteristics to the DRC observed for a tornado on June 6, 2005 (Kennedy et al. 2007). The DRC appears to be slightly split, with an area of precipitation descending vertically, and a second descending diagonally to the base of the Bennington tornado. Video analysis using slow motion was done to estimate the direction of streamlines associated with the precipitation within the DRC (upper second panel). In the image, the nose of the DRC has just arrived at the RFD occlusion, and the Bennington tornado has just begun.

In the lower left panel, the 0.5 degree reflectivity scan from KTWX shows the Bennington supercell 26 seconds after the tornado start time. The DRC is located from south-southwest to east of the tornado. In the video captures, the DRC is evident by the dark gray appearance to the left of the tornado (upper two right panels and lower two middle panels). A parade of three vortices is located just to the southeast of the tornado on the DRC's inside edge (upper third panel). In the image, these vortices are moving northeastward along the northwest edge of the DRC's leading core. This area is highlighted on the radar image (lower left panel). Vortices associated with the DRC continued to generate periodically for over 90 seconds while the DRC interacted with the tornado. The fourth vortex is shown in the upper right panel, one minute after the tornado start time. A fifth much larger vortex is evident at the surface immediately south of the tornado in the lower second panel. A sixth vortex is located higher up in the lower third panel. This vortex is lighter than the tornado, having a light gray appearance. The panel to the lower right shows the Bennington tornado just over two minutes into its life, with the DRC absent. At this point, the DRC has been absorbed into the tornado, and is no longer impacting tornado development.

The Bennington case shows that the DRC can generate vorticity along its edge. Vortices associated with DRCs appear to be common in time-lapse videos of high-end tornadoes. In the Bennington tornado example, these vortices are located on the edge of the downdraft within the RFD, dispelling the idea that these type of vortices are only generated on the forward flank of the supercell.

This visual observation supports the study's hypothesis that the tornado begins nearly simultaneously with the DRC's arrival. It must be noted that while the Bennington tornadic supercell was very close to the 208 case average concerning the DRC, many cases vary from this timing. The higher winds within the DRC can gust out ahead, reaching the RFD occlusion before the reflectivity gradient gets there. In other cases, the higher winds within the DRC remain back further to the west inside the DRC's reflectivity max, with the DRC's reflectivity gradient reaching the RFD occlusion ahead of the high winds.

Figure 14. Tornadogenesis associated with the Bennington, Kansas EF3 tornado on May 28, 2013. The video was taken by Brian Barnes, the lead forecaster of StormTours.com. Each video capture looks northwest with the time during the tornado in the upper right corner. In the two upper left panels, the DRC can be seen to the left of the Bennington tornado, which has just begun. While subtle, the DRC appears split with one nearly vertical column and another diagonal segment, which extends to the base of the tornado. The radar image at the lower left shows the hook of the Bennington supercell. In the radar image, the area where a parade of vortices developed in response to the DRC, is outlined just southeast of the tornado. The two upper right panels and two lower middle panels show six vortices that formed near the DRC's inside edge within this highlighted area. In the lower right panel, the Bennington tornado can be seen nearing full strength at about two minutes into the tornado's life. The DRC is absent after being absorbed into the tornado. The DRC is no longer impacting tornadogenesis, evident by a lack of precipitation left of the tornado.

This DRC arrival process is shown in Figure 15 for the Moore, Oklahoma EF5 tornado on May 20, 2013. The Moore tornado develops in panel 4, first at the surface as the DRC hits the RFD occlusion. This process in which the tornado develops at the surface first or within a column all at once, is theorized to be true of all tornadoes (Houser et al. 2018). In addition to the DRC in light gray, the occlusion downdraft is in dark gray. The occlusion downdraft appears to have been first mentioned in Fujita 1975, but is also covered in Klemp and Rotunno 1983, Markowski 2002, Davies-Jones 2006, Lee et al. 2011 and Lee et al. 2012. The best observation of an occlusion downdraft was made on April 9, 2015 during the Rochelle, Illinois EF4 tornado. In the video, the occlusion downdraft is seen down the road to the left (1 minute 29 seconds into the video), where strong downward motion is observed on the tornado's leading edge (youtube.com/watch?v=OEqJ2HKR5sE). The occlusion downdraft is likely a relatively steady state feature that develops in response to the DRC as the tornado begins.

Figure 16 shows the entire sequence of events that contributed to the development of the Joplin, Missouri EF5 tornado on May 22, 2011. The Joplin storm had many features hypothesized to be important for tornadogenesis, including the RFD surge, DRC, cell mergers, inflow connection and inflow channel, which made it ideal for studying and understanding tornadogenesis. The Joplin supercell's DRC arrival process for tornadogenesis was very similar to the supercells for the Moore EF5 and Bennington EF3 tornadoes. All three were representative tornadogenesis cases.

DRC and Occlusion Downdraft of the Moore, OK EF5 Tornado on May 20, 2013

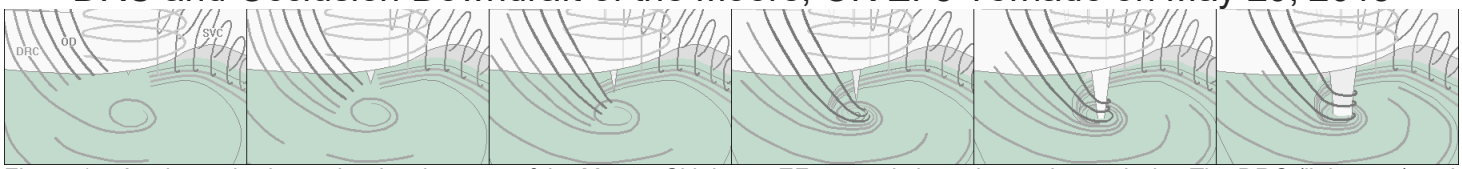

Figure 15. A schematic shows the development of the Moore, Oklahoma EF5 tornado based on radar analysis. The DRC (light gray) and occlusion downdraft (dark gray) descended to the surface immediately prior to the start of the tornado. The tornado began shortly after the DRC and occlusion downdraft wrapped into the RFD occlusion. The tornado rapidly strengthened to EF4, two minutes after forming.

For the Joplin case in Figure 16, a storm approaches the western side of the Joplin supercell (upper left in panel 1). Further to the south in panel 2, a cell of less than 50 DBZ rapidly initiates and begins to merge with the western edge of the Joplin supercell's pendant. At this time, the pendant remains straight, which signals that the RFD surge has not yet begun. The first cell merger with the pendant, continues in panel 3, instigating the RFD surge. The RFD surge begins to advance south-southeastward toward the southern edge of the mesocyclone. To the north of the meso in panel 3, an inflow notch is evidence that the RFD surge has begun. The storm to the north, merges into the western part of the pendant, constituting cell merger two. This reinforces the RFD surge. Cell merger one is completed by panel 4, which then results in the initiation of the DRC. The DRC forms to the northwest of the RFD occlusion (white circle). The DRC hits the RFD occlusion in panel 5, and the tornado begins. The RFD surge continues to move eastward, as another cell merger becomes imminent to the southwest. In panel 6, the tornado strengthens on the north side of the DRC within a curved cavity. A third cell merger occurs. The RFD surge and DRC move past the strengthening tornado on the south side, with the DRC being partly absorbed into the tornado.

DRC and Cell Mergers Associated with Formation of Joplin, MO EF5 (May 22, 2011)

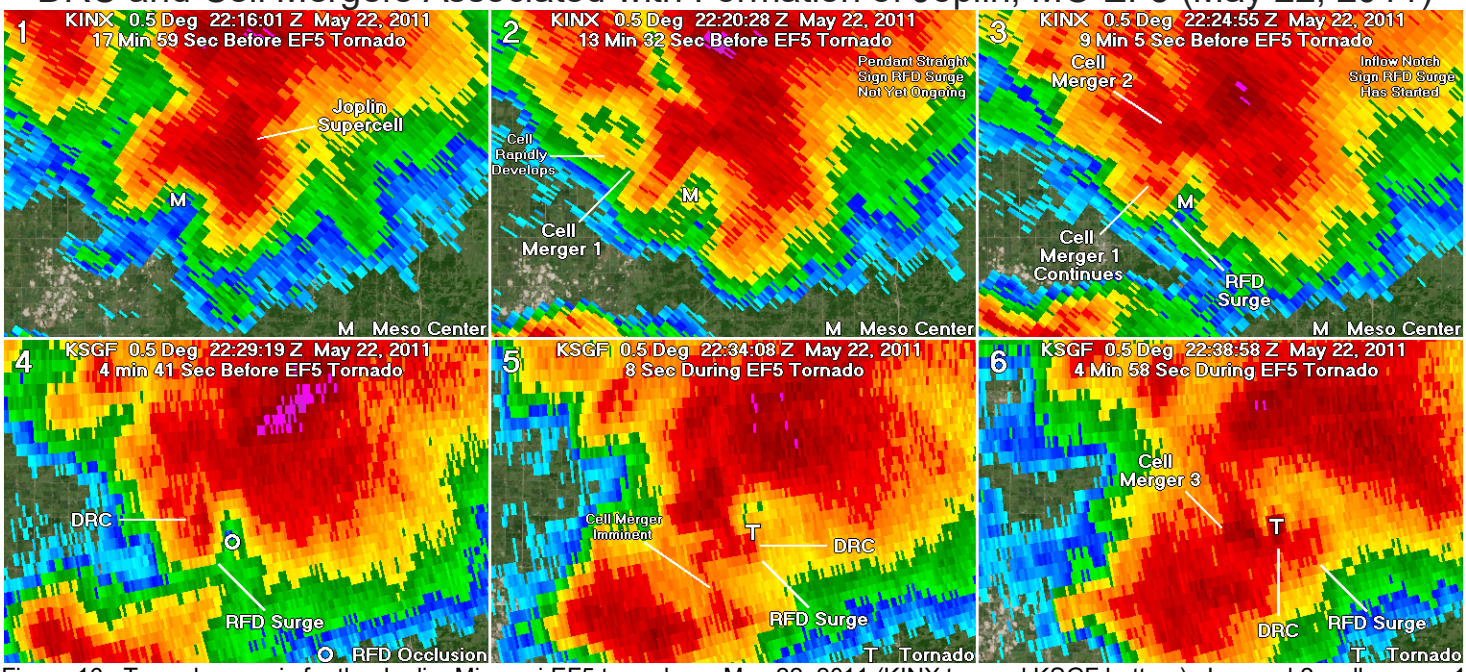

Figure 16. Tornadogenesis for the Joplin, Missouri EF5 tornado on May 22, 2011 (KINX top and KSGF bottom). In panel 2, cell merger 1 occurs with the west edge of the Joplin supercell's pendant. This cell merger instigates the RFD surge (panel 3) and enables DRC formation (panel 4). The RFD occlusion develops on the RFD boundary, south of the inflection point (panel 4). The RFD surge (Type 2) and DRC (Type 1) move south-southeastward on the RFD occlusion's west side (panel 4). The RFD occlusion is absorbed into the RFD (panel 5). The DRC's nose wraps into the RFD occlusion and the tornado forms (panel 5). This is a case representative of high-end tornadogenesis.

Figure 17 shows the complete cycle of tornadogenesis for the Hattiesburg, Mississippi EF3 tornado on January 21, 2017. The Hattiesburg tornado is an excellent case showing features hypothesized to be important for tornadogenesis, with a cell merger, RFD surge, RFD occlusion, DRC, inflow channel and streamwise vorticity current (SVC). The SVC will be covered in section 6.

In the analysis, the RFD surge appears to be instigated by outflow from an approaching cell just prior to the cell merger into the supercell's southwest flank. The RFD surge creates the inflow channel, which coincides with SVC formation. Near that time, the cell merger aids development of the DRC, southwest of the RFD occlusion. The RFD boundary moves further away from the RFD occlusion as the DRC approaches from the southwest. The tornado forms as the nose of the DRC wraps into the RFD occlusion.

Shortly before tornado formation, a circulation develops near the RFD boundary just to the southeast of the inflection point. This inflection point circulation moves southward and is absorbed into the RFD. The circulation merges with the tornado about five minutes after the tornado start time, which markedly strengthens the tornado. By this time, the inflow channel has lengthened and a fully developed SVC is in place.

4. FINAL CONSIDERATIONS

This study found that DRCs are almost always associated with tornadogenesis at the high-end, and that the tornado forms when the DRC wraps into the RFD occlusion. However, it must be made clear that these DRCs sometimes occur in high-end tornadic supercells apart from tornadogenesis, and they can occur in non-tornadic supercells (Kennedy et al. 2007).

Rasmussen et al. 2006 found that some supercells produce DRCs prior to low-level mesocyclone and tornado formation, some supercells produce DRCs that are associated with low-level rotation but not associated with tornadogenesis, and some supercells do not produce DRCs, and as a result, do not have low-level mesocyclone intensification. If the low-level mesocyclone is not strong enough or the RFD occlusion is not established, then the enhancement of low-level rotation associated with a DRC, will not be sufficient for high-end tornadogenesis.

Complete Cycle of Tornadogenesis for Hattiesburg, MS EF3 on January 21, 2017

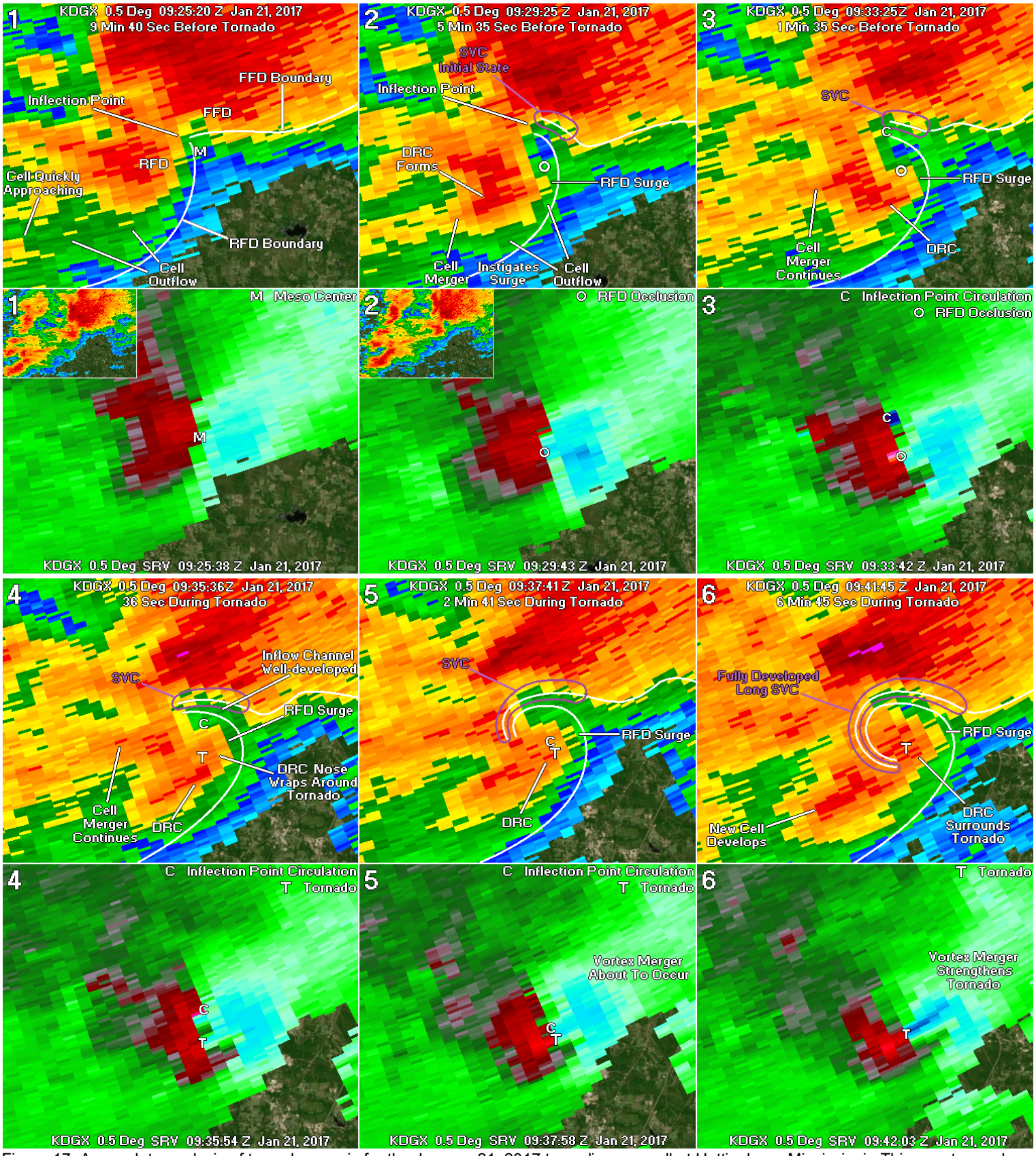

Figure 17. A complete analysis of tornadogenesis for the January 21, 2017 tornadic supercell at Hattiesburg, Mississippi. This event was close to the 208 case average. In panel 2, a cell merger and associated outflow instigate the RFD surge and DRC. The RFD surge pushes into the inflow sector of the supercell (panel 2 and 3), creating the inflow channel and SVC, discussed extensively in section 6. The nose of the DRC approaches the RFD occlusion from the southwest and wraps into the circulation just as the tornado starts (panel 4). A second circulation develops near the RFD boundary to the southeast of the inflection point (panel 4). This circulation is absorbed into the RFD, merging with the tornado about three minutes after the tornado start time, markedly strengthening the tornado (panel 5 and 6).

5. INFLOW CHANNEL

For analyzing the 208 supercells, a method was created to identify the inflow channel. The method involved three thresholds to increase objectivity. First, the inflow channel must be longer than it was wide. Second, the inflow channel must have a reflectivity difference of greater than 4 DBZ from the center to the edges. Third, the inflow channel must have time continuity. If an inflow channel was found using these criteria, then the start time, end time and duration were recorded on the spreadsheet.

The organization of the forward flank was found to be important for inflow channel development. It was observed that a strong gradient of reflectivity would develop when the forward flank became organized. This signified the presence of strong downward motion on the downdraft side of the precipitation gradient. For this study, the inflow side of the precipitation gradient was determined to be the ideal location for the forward flank downdraft (FFD) boundary. This agrees with some studies including the first to propose this location, Klemp and Rotunno 1983. Other studies have found the FFD boundary starts in the supercell's main downdraft and cuts diagonally across the forward flank precipitation gradient, crossing the far northwestern part of the supercell's inflow sector (Schueth et al. 2021). While some storms could have an FFD boundary in this location, another plausible location is along the updraft-downdraft interface, mentioned in Kosiba et al. 2013. This interface runs parallel to the forward flank precipitation gradient, from northeast to northwest of the mesocyclone extending southward and then southeastward along the eastern edge of the hook. A more occluded RFD, like is often seen on radar, would likely result in an FFD boundary position further north and west along this interface.

Davies-Jones et al. 2001 lists the three types of supercells as low precipitation, classic and high precipitation. While supercells that are low precipitation may have an FFD boundary that begins under the supercell's main downdraft, that type is not usually associated with EF3 to EF5 tornadoes. We have found that most high-end tornadic supercells are on the wet end of classic, meaning that heavy precipitation is located within the supercell's main core, including along its forward flank. Once precipitation increases enough, air near the surface is modified. A boundary is then created along the edge of the heavy precipitation, where there is a thermal and moisture gradient. Some supercells in our database likely have two boundaries, with one along the forward flank precipitation gradient and another further back in the forward flank downdraft. This was found to be the case for one supercell analyzed by Schueth et al. 2021. But for high-end tornadic supercells, most often they are on the wet end of classic, which makes the forward flank precipitation gradient the most likely location for a prominent FFD boundary. We use 35 DBZ as a guide for placing the FFD boundary.

Once an FFD boundary is established by the supercell, the stage is set for the development of an inflow channel. All that is needed is for the rear flank downdraft (RFD) surge to push eastward and northward toward the FFD boundary. When the RFD surges at a speed faster than the parent supercell, inflow coming toward the supercell from a southeasterly direction is partially blocked. As the RFD boundary approaches the FFD boundary, inflow air is forced to go around the block into the area where the RFD and FFD boundaries are parallel. This narrow corridor is called the inflow channel.

After analysis was done for all 208 supercells, the time of inflow channel development was found relative to the tornado start time. For the 208 case average, the inflow channel began about 5 minutes before the tornado start time. The inflow channel's end time was almost 16 minutes after the tornado start time, with a duration of about 21 minutes.

For 25 cases, the inflow channel was examined at the lowest elevation angle in much greater detail shortly after the RFD occlusion's maturation time. The inflow channel's documented characteristics included direction and distance to the RFD occlusion, minimum width, and maximum internal wind speed. To determine the maximum wind speed within the inflow channel, the base velocity image shortly after the RFD occlusion matured, was examined for the 14 highest confidence cases. The bin with the highest inbound or outbound wind speed within the inflow channel was recorded. The direction of the wind was estimated based on the orientation of the inflow channel. Wind likely flows parallel to the inflow channel for much of its length because wind direction largely determines the inflow channel's orientation. This direction was estimated and then subtracted from the direction of the beam. The angle difference was used in a calculation to adjust the inflow channel's wind speed upward. If the wind direction was estimated to be parallel to the beam, then no adjustment was made. But if it was not, the wind speed was adjusted more and more as the angle increased.

The same procedure was done across the inflow sector of the supercell. A bin was chosen away from the inflow channel that appeared to be in an area where wind speeds were relatively similar and close to the inflow sector's average. The surrounding fourteen bins were averaged for the bin selected to find the average wind speed. And then, the difference between the estimated inflow sector wind direction and beam direction was found. The adjustment equation was again used to make the wind speed adjustment. The following table presents the results of the inflow channel investigation.

Inflow Channel Characteristics

For High Confidence Cases

Inflow Channel Start, End and Duration Times - 208 Cases

Start Time	5 min 21 sec	Before Tornado
End Time	15 min 51 sec	After Tornado Start Time
Duration	21 min 12 sec	

Inflow Channel Avg. Direction/Distance from RFD Occlusion
1.07 Nautical Miles (1.98 Km) at 9.4 Degrees - 25 Cases

Average Width of Narrowest Section Within Inflow Channel
0.45 Nautical Miles (0.83 Km) - 25 Cases

Inflow Channel Estimated Average Maximum Wind Speed
72.62 Knots - 14 Cases

Estimated Average Wind Speed of Supercell's Inflow Sector
34.33 Knots - 14 Cases

Average Percent Wind Speed Increase Within Inflow Channel
111.54% - 14 Cases (Avg Elevation 3,257 Ft)

This dramatic increase of wind speed within the inflow channel is due to the Bernoulli Effect, which the Smithsonian National Air and Space Museum defines as the following.

The Bernoulli principle is a restatement of the conservation of momentum. The energy of a stream of air is shared between pressure energy (due to random molecular collisions) and stream flow energy (the shared component of the molecular motion in the direction of the stream). As the air moves around an object, it is forced to speed up because of mass conservation. The stream flow energy thus increases, and since the total amount of energy has to remain constant (energy conservation), this must come at the expense of the random molecular energy or pressure. Therefore, the pressure must drop the faster the air stream is accelerated.

This is important to tornadogenesis because air from the inflow sector speeds up as it enters the supercell's inflow channel. A sharp pressure drop occurs within the inflow channel, before this fast-moving air rises into the low-level mesocyclone, strengthening rotation.

6. STREAMWISE VORTICITY CURRENT

As more was learned about the inflow channel, it was theorized that the streamwise vorticity current (SVC) is strongly related to the inflow channel. It was noticed during analysis, that for almost all the high-end tornadic supercells, the strongest reflectivity gradient along the forward flank developed coincident with the formation of the inflow channel. And after studying the inflow channel in more detail, it was determined that the FFD boundary was most often located near the forward flank precipitation gradient, starting at the inflection point, where the RFD and FFD boundaries converge. The inflection point can be a place where smaller circulations develop within the mesocyclone. But these circulations appear to be more related to the bend in the precipitation shaft than the SVC because they most often remain anchored to the inflection point and are vertically stacked.

The FFD boundary usually extends outward over five miles, and sometimes over ten miles, along the forward flank precipitation gradient. As was found in Schueth et al. 2021, the strongest horizontal vorticity is likely generated along and north of the FFD boundary. Our study proposes that the SVC is located from the forward flank side of the inflow channel, extending westward along the forward flank precipitation gradient, and then southwest, south and southeastward along the eastern edge of the hook echo. We propose that a well-developed SVC wraps cyclonically around the eastern edge of the supercell's hook until it reaches the area just southwest of the tornado. This is substantiated by case studies that will be shown in detail later in the paper.

The schematic in Figure 18 shows our proposed location of the SVC (orange) as determined by this study. Also shown are locations of the inflow channel (green), RFD (red), FFD (blue), updraft (tan) and tornado (T). This is a fully developed SVC at the violent tornado stage. The graphic was adapted from Lemon and Doswell 1979.

Our conclusion is different than some computer model simulations, which show that the SVC cuts directly across the inflow sector to the north of the tornado (Orf et al. 2017). We believe the reason for this difference is that these computer simulations may not have simulated the RFD correctly. In some computer simulations during tornadogenesis, the RFD does not surge toward the forward flank. The RFD stays back west or southwest of the tornado. The horizontally oriented circulation that is generated along the FFD boundary in these simulations is not affected by the RFD, thus it can travel across the inflow sector to the north of the tornado. This is not representative of what our observational analysis of high-resolution radar data has shown.

In radar data, the RFD surges north and east toward the forward flank, creating the inflow channel. The SVC develops coincident with the inflow channel because inflow channel wind speeds approximately double due to the Bernoulli Effect. In response to this dramatic increase in inflow, updraft speeds accelerate, which create and sustain the southern edge of the SVC. Other studies, such as Orf et al. 2017, have also found that the SVC is strengthened by increasing inflow. In our study, rapid downward motions associated with heavy precipitation in the forward flank downdraft create the northern edge of the SVC. While an SVC can form in non-tornadic supercells (Murdzek et al. 2020), the strongest and most developed are often associated with high-end tornadic storms.

Various Features of a Violent Tornado Producing Supercell

Fully Developed SVC, Inflow Channel, RFD, FFD, Updraft

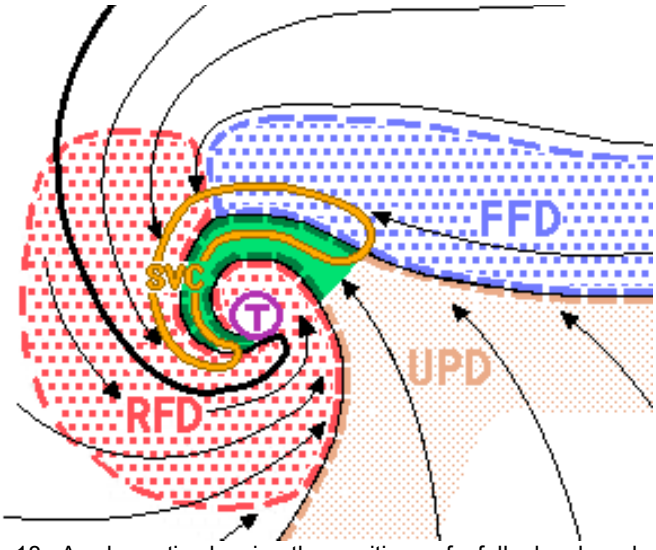

Figure 18. A schematic showing the positions of a fully developed tornadic SVC (orange), inflow channel (green), RFD (red), FFD (blue) and updraft (tan) of a tornadic supercell (adapted from Lemon and Doswell 1979). Streamlines are at 300 meters.

The reason is that high-end tornadic supercells have been observed to generate very strong inflow wind speeds. The inflow channel appears to be the cause of the highest wind speeds, supporting our idea that the inflow channel and SVC are related.

Concerning the timing of SVC development, the start and end times would likely coincide with the inflow channel. For the 208 case average in our database, the SVC would start about 5 minutes prior to the tornado start time. Similarly, Dixon et al. 2018 and Orf et al. 2018 found that the SVC in the simulated EF5 El Reno, Oklahoma tornadic supercell on May 24, 2011, began several minutes before the tornado started. The average SVC ending time in this study was about 16 minutes after to the tornado start time, lasting around 21 minutes on average. For a long-track tornado lasting longer than the average duration time, a temporary breakdown of the inflow channel and SVC may not result in a dissipation of the tornado.

In most cases, the strongest generation zone of horizontal vorticity is likely near the FFD boundary in a northward direction from the tornado (supported by Schueth et al. 2021). This would make the FFD boundary's orientation, compared to the environmental flow going over the inflow channel, most favorable for the generation of horizontal vorticity. Wicker 1996 and Shabbott 2006 suggested the relative orientation of the baroclinic vorticity produced in the FFD outflow to the mean vertical shear, would control how much total horizontal vorticity is ingested by the updraft. Our hypothesis suggests that this horizontal vorticity is generated and carried downstream, eventually turning southward and then southeastward around the precipitation gradient along the inner part of the hook.

From looking at tornadic supercells on radar, often there is a sharp bend at the inflection point, where the RFD and FFD boundaries converge. We hypothesize that this can potentially disrupt the SVC, as is shown in Figures 19 and 20. The position of maximized horizontal vorticity generation is shown for each case upstream of the inflection point, similar to a graphic in Schueth et al. 2021. In both cases here, the RFD and FFD boundaries end at the inflection point, where the angle within the precipitation gradient exceeds 90 degrees. This sharp angle likely cuts off the SVC.

RFD and FFD Boundaries, Inflection Point and SVC

Bowdle, SD EF4 - May 22, 2010

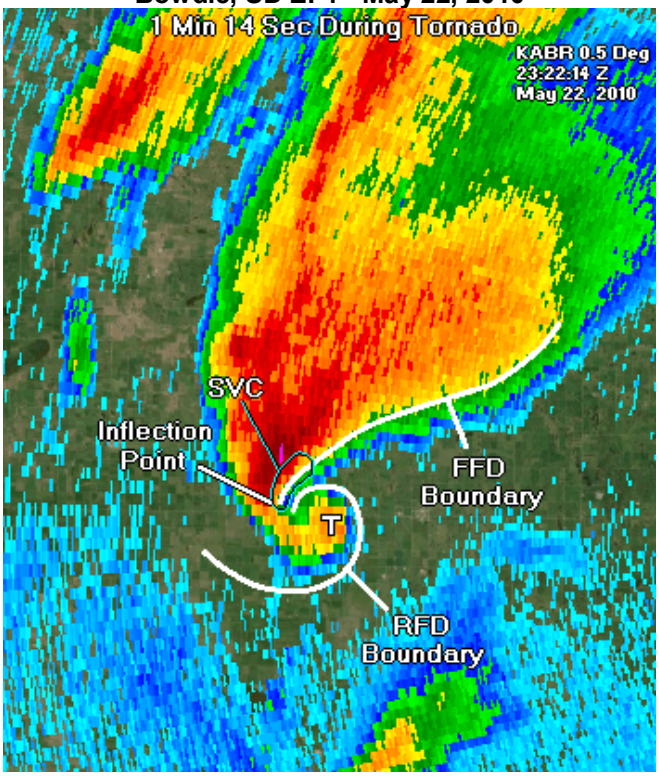

Seminole, OK EF3 - May 10, 2010

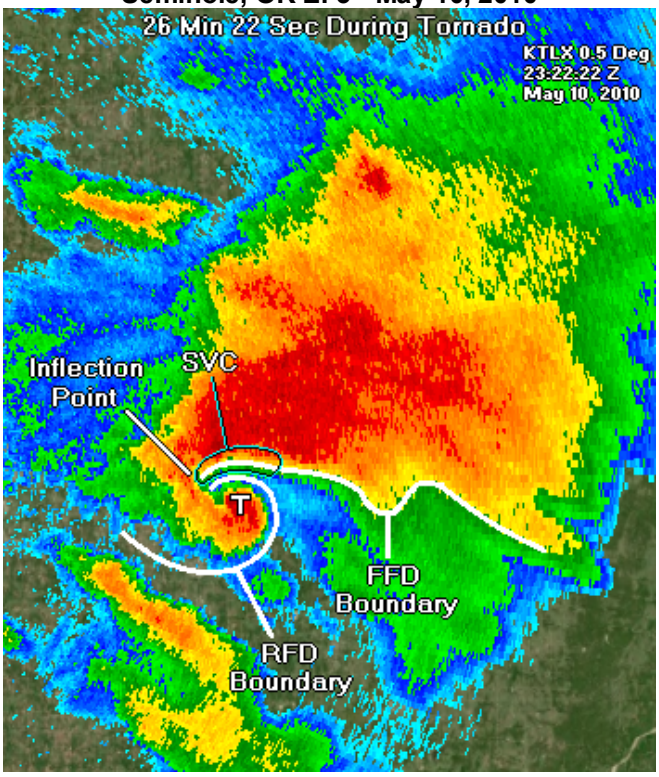

Figures 19 and 20. The two examples above show the location of maximized horizontal vorticity generation within the SVC. The sharp angle created at the inflection point, where the RFD and FFD boundaries converge, can likely be disruptive and cut off the SVC. The SVC appears to not be fully developed in these two cases.

The schematic in Figure 21 shows the mechanics of the SVC, highlighting the importance of the inflow channel to the SVC. As the inflow channel forms, winds dramatically increase within this narrow corridor, which is hypothesized to be coupled with a pressure drop and an acceleration of updraft speeds. Environmental air that does not enter the inflow channel is forced to go up and over the top of the inflow channel. Eventually, this rising air reaches the forward flank downdraft to the north of the FFD boundary, which causes the air to turn down and rapidly descend to the ground. When the air reaches the ground, it is drawn back toward the inflow channel, where the pressure has dropped due to the Bernoulli Effect. This completed rotation generates the SVC. The SVC will persist as long as the inflow channel remains in place.

Mechanics of the Streamwise Vorticity Current in a High-end Tornadic Supercell

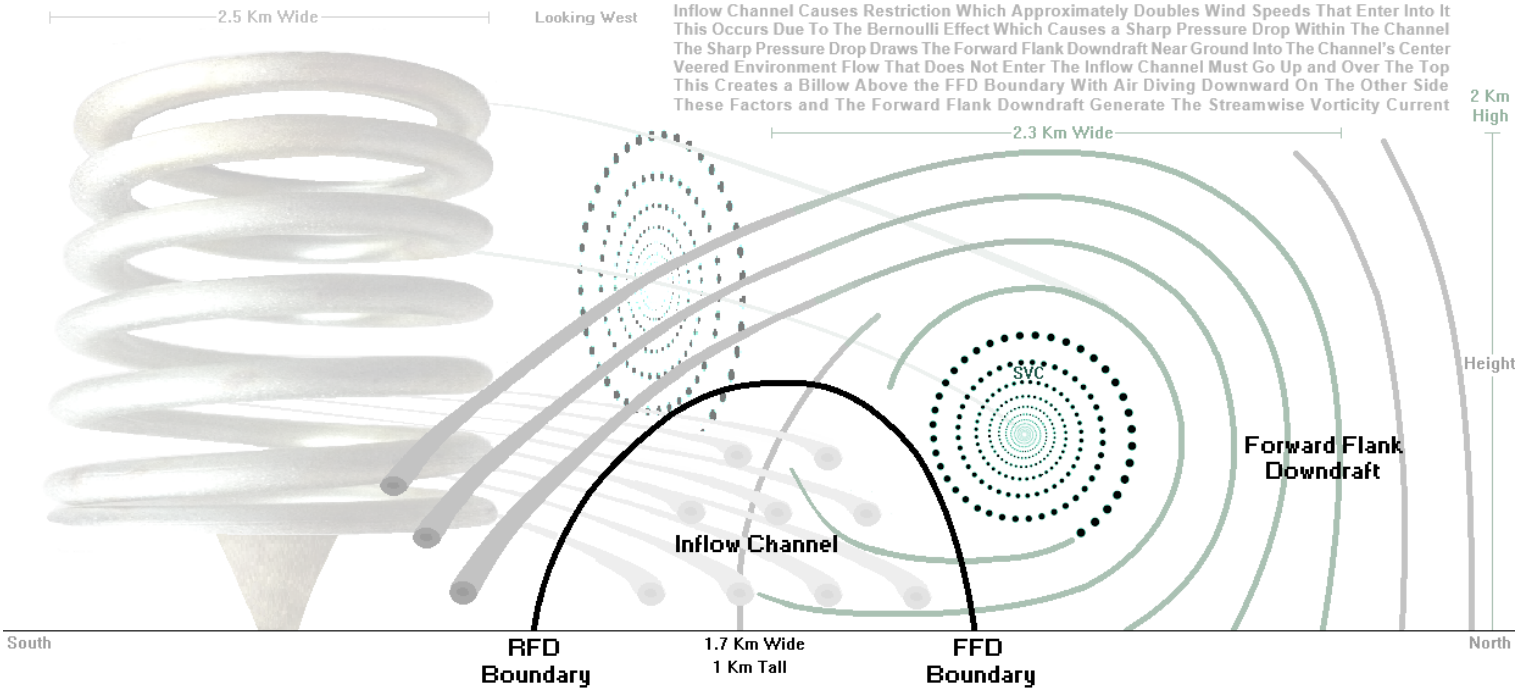

Figure 21. A schematic is shown looking down the inflow channel toward the west. The low-level mesocyclone is on the left side of the drawing. The position of the SVC, according to this study, is shown relative to the inflow channel and forward flank downdraft.

There has been a suggestion that the WSR-88D high-resolution radar is inadequate for the examination of features such as the SVC. For our database, near the center of the RFD occlusion, the average bin size for the top 10 supercells closest to the high-resolution radar was 797 feet by 378 feet. In one of our case studies further on in this paper, an SVC-supported circulation that was detected by high-resolution radar was estimated to be just above the minimum detectable threshold, at 600 to 800 feet in width. And for most cases, the inflow channel is over 4,000 feet in diameter, while for those same cases, our study suggests that the SVC is over 5,000 feet in diameter. These dimensions indicate that some SVCs can be detected using high-resolution radar. While the WSR-88D may not be ideal for observing these features, the WSR-88D radar should not be ruled out for detecting larger SVCs.

To determine the impact that a forward flank circulation would have on the RFD occlusion, a spatial comparison must be made. It was difficult to determine an average width for the RFD occlusion because many cases had a broad rotational component within the RFD's northeast quadrant during tornadogenesis. For many cases, rotation strength was observed to gradually increase toward the center of the RFD's northeast quadrant, where the RFD occlusion is often located. Our study estimated that a matured RFD occlusion, on average, is approximately just under a nautical mile in width or about 5,000 feet in diameter. If we consider a merging circulation from the forward flank, just below the detectable threshold at 450 feet in diameter, that circulation would merge with the RFD occlusion that is about an order of magnitude larger in size. While some impact likely would be made, it would probably be minimal.

Then, there is the problem with timing. For the 208 supercells in our database on average, the RFD occlusion matured about 5 minutes prior to the tornado start time, and the inflow connection was made shortly after the tornado start time. For the average case in the database, the inflow channel and associated SVC would arrive at the tornado just over 5 minutes after the RFD occlusion matured. This suggests that the RFD occlusion would more likely be the driving process for tornadogenesis, and not the SVC.

And lastly, there is the problem of proximity. On average for the 208 supercells in our database, the inflow channel's closest point to the RFD occlusion, shortly after the RFD occlusion maturation time, was 1.07 nautical miles. The inflow channel's minimum width near that same location was 0.45 nautical miles. This study's estimate is that the SVC's southern edge starts about 60% of the way across the inflow channel going towards the forward flank. This would be 0.27 nautical miles across the inflow channel's narrowest width. Adding the distances together places the southern edge of the SVC 1.34 nautical miles to the north (9.4 degrees) of the RFD occlusion (208 case average), shortly after the RFD occlusion has matured, a few minutes before the tornado. These three issues of magnitude, timing and proximity, challenge the assertion that the SVC plays a major role in tornadogenesis.

The proposed location of a well-developed SVC is shown in Figure 22 for the EF5 supercell at Moore, Oklahoma on May 20, 2013. The inflow channel and associated SVC are high-end, with the SVC location analyzed along the FFD precipitation gradient to the north and west of the tornado.

Fully Developed SVC for the Moore, Oklahoma EF5 Tornado on May 20, 2013

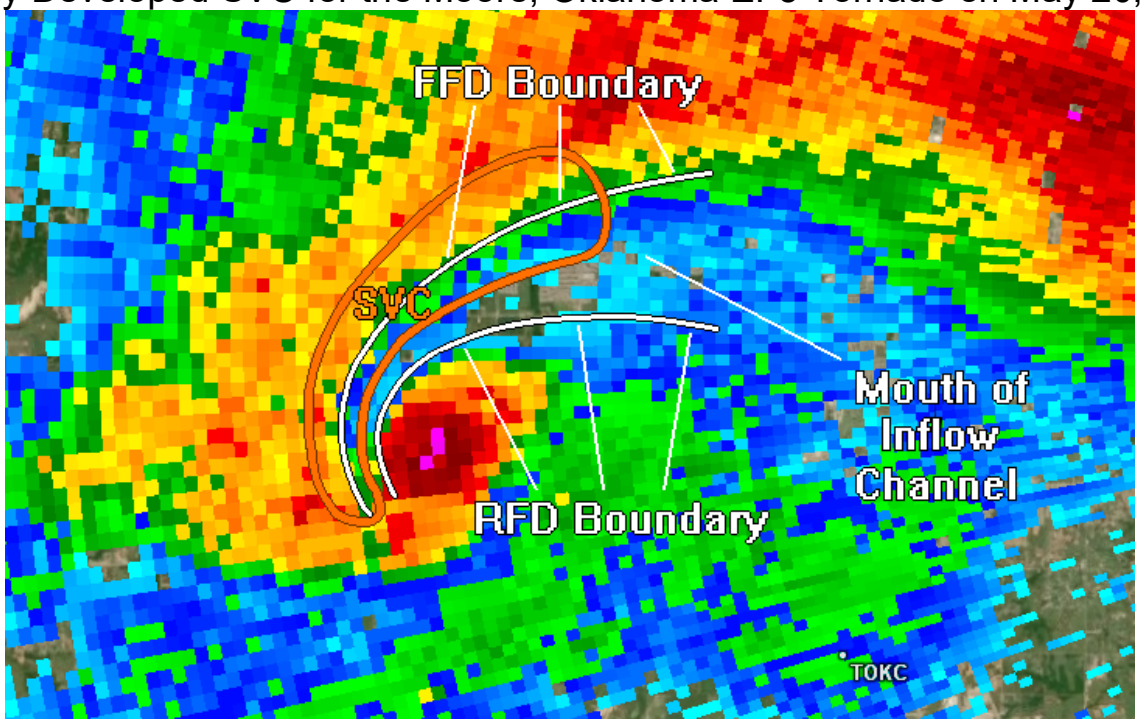

Figure 22. The estimated location of the well-developed SVC for the Moore, Oklahoma EF5 supercell on May 20, 2013, as determined by radar analysis from this study.

A convective seminar (Satrio 2022) entitled "A Triple-Doppler Analysis of the 17 May 2019 McCook / Farnam, NE Tornadic Supercell Sampled during TORUS", identified a well-developed horizontal vorticity circulation associated with an SVC. In his study, triple Doppler analysis shows the SVC within the forward flank downdraft, adjacent to an inflow channel. This gives us confidence in our hypothesis that the inflow channel and SVC are co-located with one another and have a close relationship.

After looking at the Satrio 2022 triple Doppler analysis of the SVC and coupling that with our study of the inflow channel using high-resolution radar, the SVC is approximately 130 percent of the width of the inflow channel. While supercell inflow channels vary considerably in width, an inflow channel 1.7 kilometers wide (Figure 21) would generate an SVC approximately 2.3 kilometers wide. Figure 23 shows how the size of the SVC likely varies depending upon how wide the inflow channel is, according to this study's analysis.

How Inflow Channel Width Impacts SVC Size

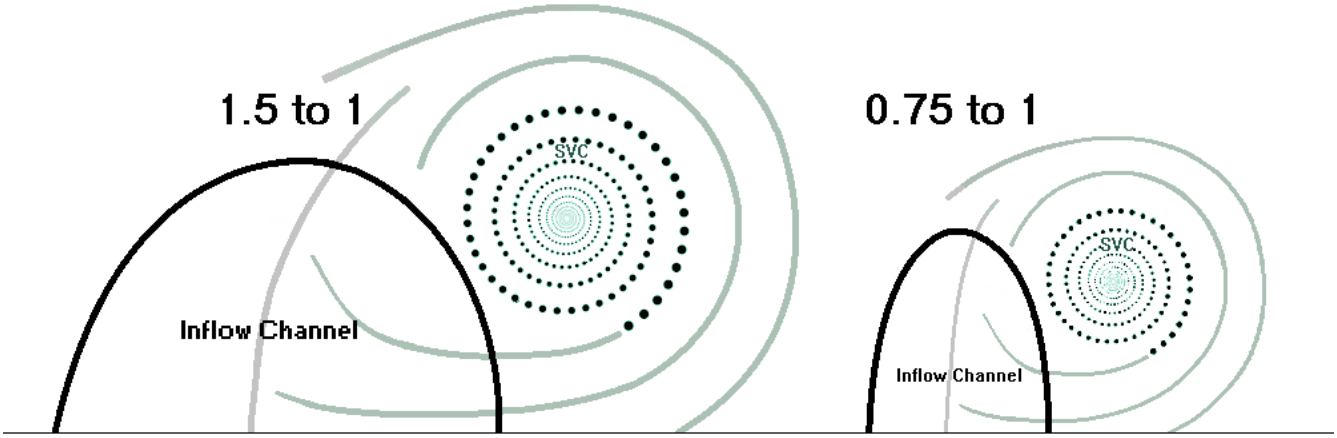

Figure 23. Although there are various setups, the size of the SVC likely depends on the width of the inflow channel. A wide inflow channel would likely generate a large SVC, while a narrow inflow channel would likely create a much smaller SVC.

When the inflow channel and SVC develop, the low-level mesocyclone likely strengthens dramatically. When horizontal vorticity rises into the updraft, the low to mid-level mesocyclone has been shown to strengthen (Peters et al. 2020). In our hypothesis, this is the primary role of both features. Concerning tornadogenesis, strengthening the low-level mesocyclone is an important factor because the mesocyclone must be strong enough to stretch the column of vertical vorticity into a tornado. For the SVC to be a significant part of strengthening the RFD occlusion near the surface, our estimates suggest that the SVC would need to be within proximity of the tornado at least one minute prior to the start of the tornado. Our analysis shows an inflow connection was made at least one minute before the start of the tornado for only 16 of the 208 supercells (7.7%). For these cases, the SVC could have been involved in tornadogenesis. But an SVC-related circulation was not found in those 16 cases. And there is the problem of size. A circulation smaller than the detectable size of high-resolution radar, might not make a difference compared to the RFD occlusion, which is more than a magnitude greater in size on average.

In Figure 24, the relatively large distance between the SVC and RFD occlusion is evident for four high-end tornadic supercells. On average, the time of the images was 4 minutes prior to the tornado start time. The positions are shown of the RFD occlusion, RFD boundary, FFD boundary, SVC and internal RFD dry slot. The internal RFD dry slot is a small-scale curved corridor of precipitation-free air around the RFD occlusion, not associated with the larger scale dry slot. For three of the four cases, the SVC was analyzed to be in an initial state, with the inflow channel adjacent to moderate to heavy precipitation. This proximity of the inflow channel to a strong downdraft is what contributes to strong horizontal vorticity, according to this study's analysis. For the fourth case (lower right), the inflow channel is not located along a precipitation gradient, making an SVC unlikely in that case. For the three cases, which are representative of 92.3% of the cases in the database, the SVC appears to be too far away from the RFD occlusion to have an impact on tornadogenesis, other than to strengthen the low-level mesocyclone. According to the analysis for these cases on average, the initial state SVC is located 1.46 nautical miles away from an RFD occlusion that is fully matured.

Four Classic RFD Structure Cases - Developing Inflow Channel, Initial State SVC, RFD Occlusion, RFD Boundary, FFD Boundary and Internal RFD Dry Slot

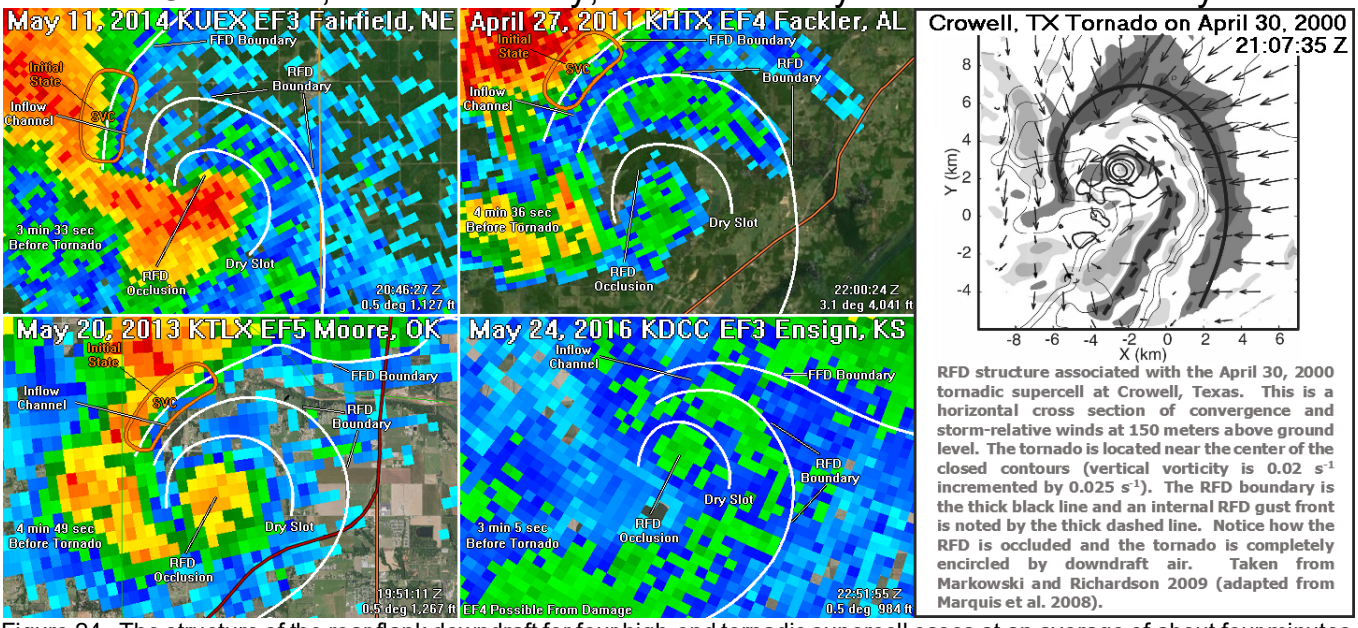

Figure 24. The structure of the rear flank downdraft for four high-end tornadic supercell cases at an average of about four minutes before the tornado start time. The four case average has the initial SVC at 1.46 nautical miles away from an RFD occlusion that is fully matured. The graphics show the locations of the RFD boundary, FFD boundary, RFD occlusion, inflow channel, SVC and internal RFD dry slot (a small-scale dry corridor associated with the RFD occlusion). This compares to the graphic at the right from Markowski and Richardson 2009 (adapted from Marquis et al. 2008).

Figure 24 also shows the RFD structure of the Crowell, Texas tornado on April 30, 2000 at 21:07:35 Z. This is an adapted graphic from Marquis et al. 2008, taken from Markowski and Richardson 2009. The RFD structure is similar to the four cases (left and middle), with the primary RFD boundary noted by the dark black line. In the graphic at the right, an internal RFD boundary is marked by the dark dashed line. The tornado is located in the circular contours within the RFD, in a similar place to the 208 case average in Figure 10 of Part 1 of this study.

The analysis of the four cases in Figure 24 differ from the April 30, 2000 case because the inflow channel on the Crowell, Texas supercell is not specifically shown. The inflow channel, for the four cases at the middle and left, is evident by the area of cleared out precipitation along the forward flank. The inflow channel is just upstream of the inflection point for each case. On average, the inflow channel and associated SVC do rapidly move toward the RFD occlusion around the start of the tornado. The 208 case average in the database shows the inflow connection was made to the southern part of the tornado about 30 seconds after the tornado start time. The inflow connection was identified by a rapid decrease of reflectivity southwest of the circulation. When the inflow connection was made, most often the tornado was already ongoing.

This study also found that the horizontal vorticity generated by the SVC can vary depending upon the inflow channel width. Figure 25 shows this relationship in a drawing for the Moore, Oklahoma EF5 tornado on May 20, 2013. Our study suggests that as the inflow channel narrows, the creation zone of horizontal vorticity also narrows. If the inflow channel is completely cut off, then the SVC will dissipate. If the inflow channel becomes reestablished, then the SVC will redevelop.

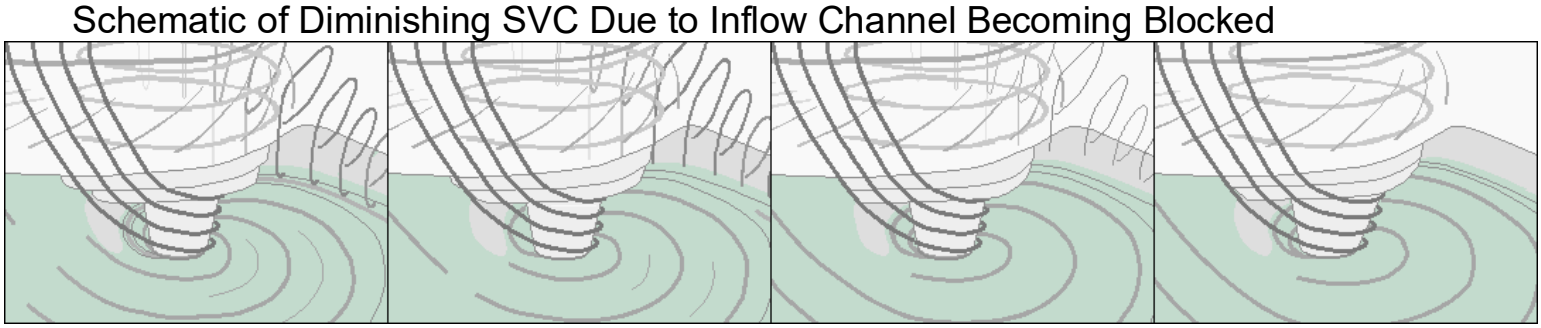

Figure 25. An illustration showing the effect on horizontal vorticity as the inflow channel decreases in width. As the inflow channel narrows, the generation zone of horizontal vorticity also narrows. Our study suggests that the SVC will dissipate if the inflow channel is cut off.

7. INFLOW CHANNEL AND SVC CASE STUDIES

In Figure 26, a case study is shown for the EF5 tornado that occurred near El Reno, Oklahoma on May 24, 2011. The case begins with the Lookeba EF3 tornado ongoing (panel 1). The SVC is already formed along the forward flank precipitation gradient. The angle of the precipitation gradient is greater than 90 degrees, likely cutting off the SVC. At this time, cells are approaching quickly from the southwest, which can also be seen in the lower right insert in the upper left panel. Cells merge with the southwest part of the hook, which causes the RFD to surge (panel 2). This lengthens the inflow channel and causes the SVC to grow. After the cell merger, the DRC forms (panel 3). At this time, the Lookeba tornado has ended and an RFD occlusion is present in the RFD's northeast quadrant.

Intense thunderstorms quickly approach the inflow channel from the south (panel 3). A very large cell merger occurs with the forward flank of the El Reno storm (panel 4). The inflow channel and SVC quickly lengthen toward the south and southeast, reaching the newly formed EF5 El Reno tornado (panel 4). The SVC is fully developed at this time and has reached a high-end state rarely observed. An SVC-supported tornado forms, approximately 1,600 feet in diameter. The SVC-supported tornado moves towards the south and then southeastward along the SVC corridor, approaching the tornado (panel 5). At this time, the distance between the SVC-supported tornado and the El Reno tornado is estimated to be around 430 feet. The El Reno tornado is likely an upper-end EF5, and has reached the maximum strength along its entire track. It has a rarely observed VROT of 120 knots (panel 5). At this time, Roger Edwards (personal communication) of the Storm Prediction Center, observed anomalously high inflow channel wind speeds, similar to what he has observed inside hurricane eye walls.

The approaching storm from the south intensifies via reflectivity along and near the RFD boundary (panel 5). As the last storm of the cell merger sequence enters the inflow channel (panel 6), the vortex merger becomes complete. The merging storm outlines the entire northwest part of the supercell's inflow sector, including the inflow channel, highlighting the RFD and FFD boundaries well (panel 6). This is a rare observance, and the only case we found of an SVC-supported tornado merging with an RFD-related tornado in the database of 208 supercells. Other detailed examinations of this case are presented in Houser et al. 2015 and Tanamachi et al. 2015. And a computer simulation of the El Reno EF5 supercell and its SVC on May 24, 2011, is presented in Orf et al. 2017.

In Figure 27, a size comparison of the SVC-supported tornado and El Reno EF5 tornado is made, when the vortex merger was imminent at 21:02:06 Z on May 24, 2011 (upper left). The radar showed the El Reno EF5 (circled in blue) at about one mile wide at its maximum strength, with a VROT of 120 knots. The SVC-supported tornado is estimated to be 820 feet wide in the radar image and is about 430 feet from the edge of the El Reno tornado (lower right). Roger Edwards of the Storm Prediction Center (SPC) witnessed this event, and his photo of the vortex merger about to take place is at the lower left. Two of Roger's photos of the El Reno EF5 tornado near maximum strength are shown at the upper right. We estimate that an event of this magnitude could be a once-in-a-multidecadal occurrence. This is the only case of this type documented in our 11½ year database. This tornado merger is also analyzed in French et al. 2015.

Tornadogenesis Analysis for El Reno, Oklahoma EF5 on May 24, 2011

Vortex Merger - El Reno EF5 Tornado and SVC-Supported Tornado

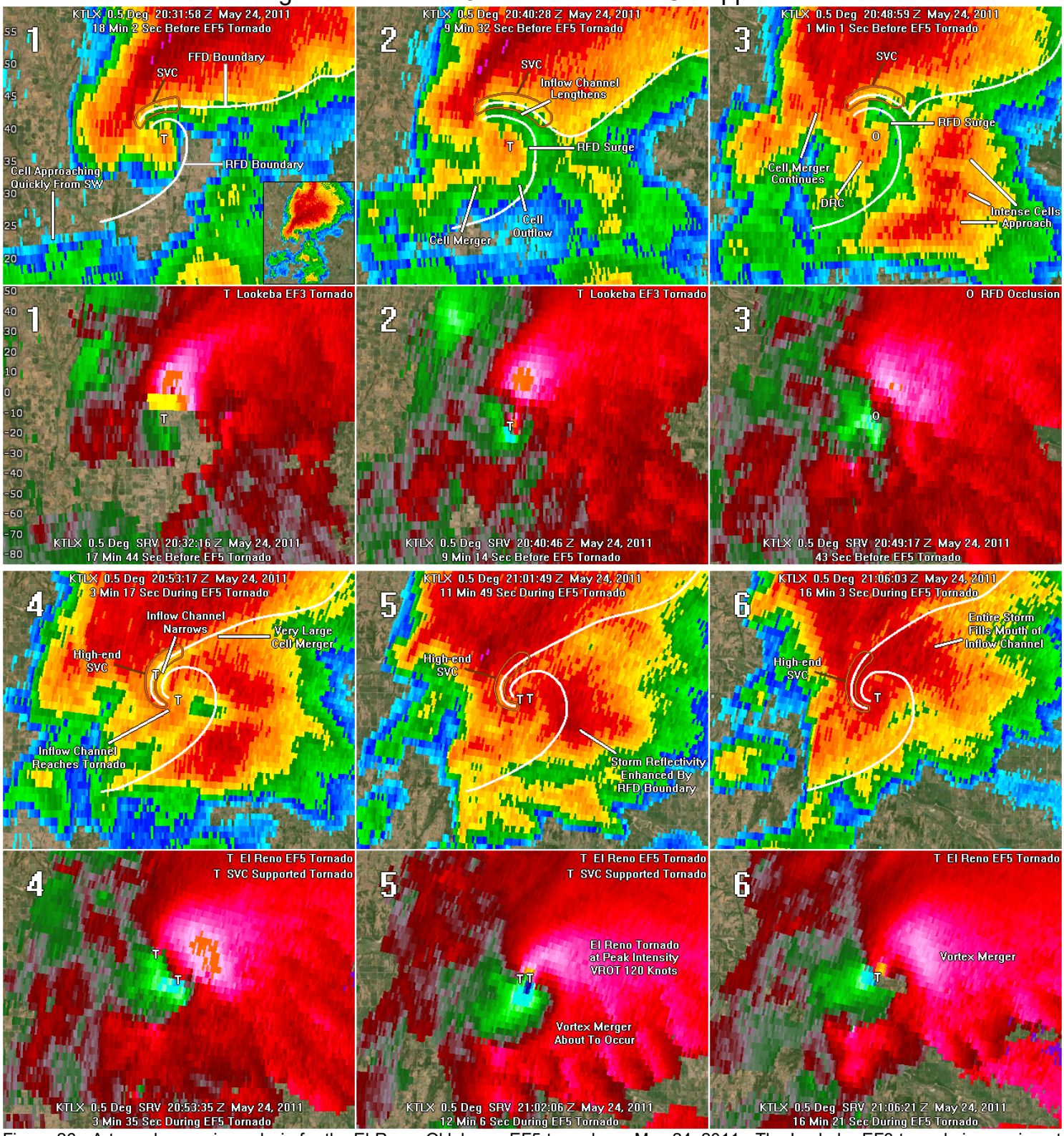

Figure 26. A tornadogenesis analysis for the El Reno, Oklahoma EF5 tornado on May 24, 2011. The Lookeba EF3 tornado is ongoing at the start of the analysis (panel 1). At that time, the SVC is located to the north and northwest of the tornado. Cell mergers occur with the southwest part of the hook, causing the RFD to surge (panel 2). This lengthens the inflow channel and SVC. The Lookeba tornado ends (panel 3) as strong storms approach the inflow channel from the south. The El Reno EF5 tornado develops (panel 4). The lead merging cell enters the inflow channel and an SVC-related tornado begins near the SVC's center. The SVC-supported tornado moves along the eastern edge of the SVC until a vortex merger becomes imminent (panel 5). The last storm in the cell merger sequence intensifies reflectivity near the RFD boundary (panel 5), before filling the inflow channel completely (panel 6). This study determined that the event sequence for the El Reno EF5 tornado was likely a multi-decadal occurrence interval.

KTLX Hi-res Radar - May 24, 2011 at 21:02:06 Z - El Reno, OK EF5 Tornado (Blue) SVC-Supported Tornado (Brown) Just Prior To Vortex Merger

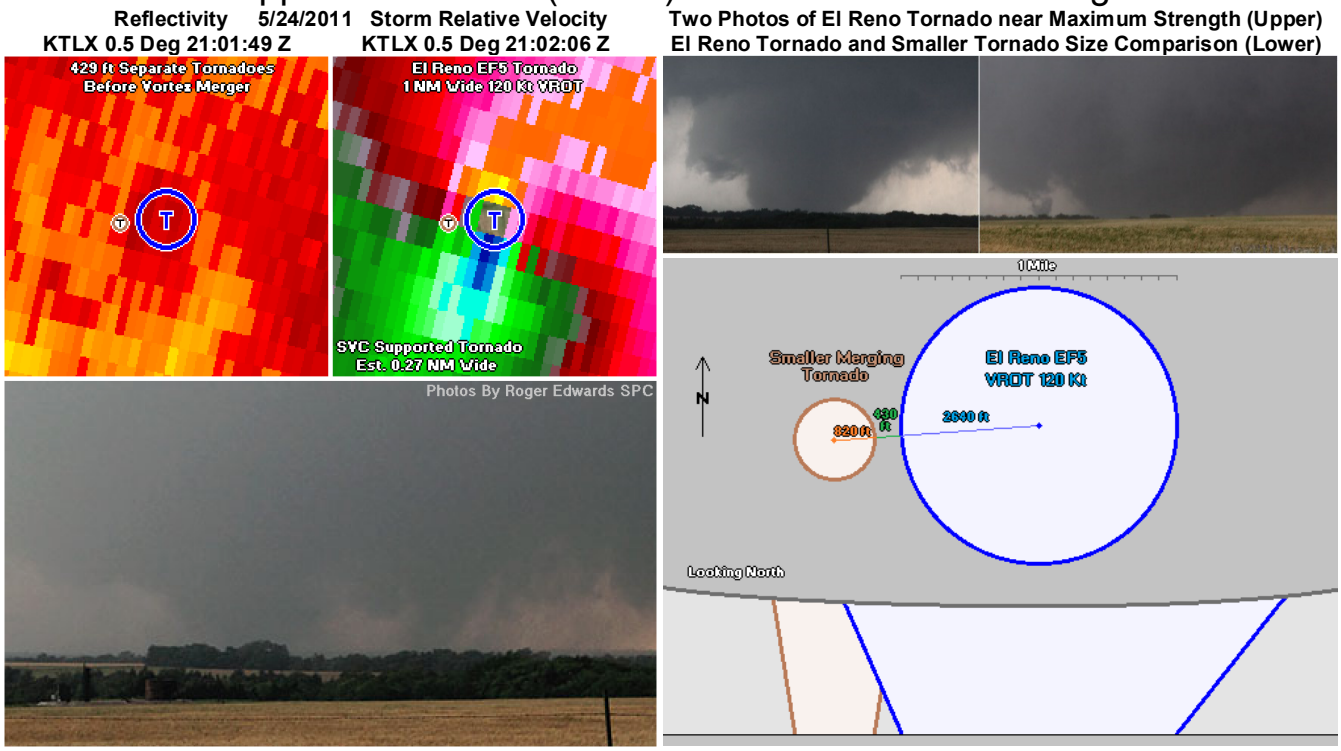

Figure 27. A vortex merger is shown at the left of an SVC-supported tornado with the EL Reno EF5 tornado on May 24, 2011. At the time of the radar images, the two tornadoes are about to merge. The imminent vortex merger is evident in the contrasted image (lower left). The El Reno EF5 is about one mile in diameter while the SVC-supported tornado is estimated at near 1,600 feet in diameter. The edges of the two tornadoes are separated by just over 400 feet (lower right). The El Reno tornado is shown in photos at the upper right near maximum strength. A satellite tornado, not associated with the SVC-related tornado, is next to the El Reno tornado at the far upper right. The three photos are by Roger Edwards of the Storm Prediction Center.

In Figure 28, the second case study is of the Bridge Creek, Oklahoma EF3 tornado on May 6, 2015. The analysis begins about 11 minutes after the tornado start time (far left panel). An inflow channel is present to the east of the entire hook, with a fully developed high-end SVC already formed. At this time, an SVC-supported circulation is observed on radar within the SVC, just to the south-southwest of the SVC's center. This circulation was estimated to be 600 to 800 feet in diameter and was just above the minimum circulation diameter of 500 feet detectable by high-resolution radar, as determined by this study. In the middle four panels, the SVC-supported circulation gradually moves southward and then southeastward down the SVC corridor. The vortex merger finally takes place (far right two panels). This path is along the eastern edge of the hook's precipitation gradient. The path never leaves the updraft-downdraft interface, as is shown in Figure 18, with the SVC encircled orange. This case and the El Reno EF5 case, are in agreement concerning the SVC position. These cases give us confidence that our placement of the SVC is correct, along the northern and western edge of the inflow channel, and along the eastern edge of the hook's precipitation gradient. Although the El Reno, Oklahoma tornado became slightly less intense after the vortex merger (Figure 26 bottom right panel), the Bridge Creek, Oklahoma EF3 tornado strengthened markedly after the SVC-related vortex merger (Figure 28 bottom far right panel).

High-end SVC and Vortex Merger - Bridge Creek, Oklahoma EF3 on May 6, 2015

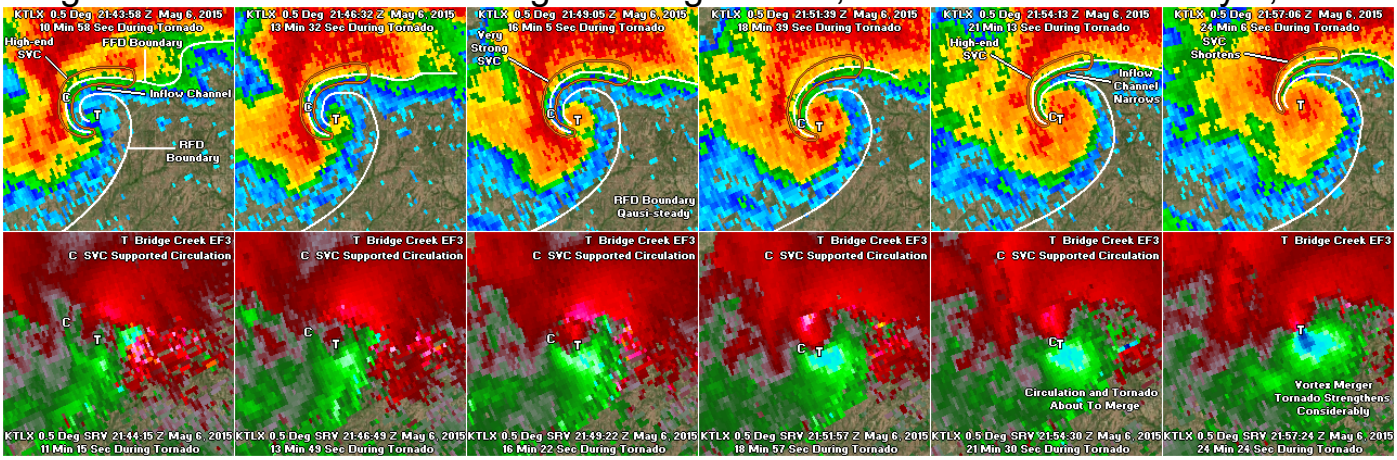

Figure 28. A vortex merger in which an SVC-supported circulation develops in a high-end SVC on May 6, 2015. The Bridge Creek EF3 tornado is ongoing (far left). The SVC-supported circulation moves southward and then southeastward along the SVC corridor, until reaching the tornado (far right two panels). The Bridge Creek EF3 tornado markedly strengthens after the vortex merger (far right). The track of this SVC-supported circulation is similar to the track of the SVC-supported tornado for the El Reno EF5 case. This gives us confidence that the study's location of the SVC is correct, along the eastern edge of the hook's precipitation gradient.

The final case study is of the tornado that occurred west-northwest of Grow, Texas on May 4, 2022. The lead author of this study was storm chasing in west Texas on that day. The mesocyclone approached his position and went directly overhead. After the mesocyclone crossed the road, a tornado developed beneath the mesocyclone just to the east of the road and close to the author's position. The storm was a classic supercell but lacked the heavy precipitation around the mesocyclone, making conditions ideal for observing tornadogenesis. The author took two time-lapse sequences. The first was from 6:32 to 6:33 pm CDT. The second was from 6:34 to 6:39 pm CDT and is associated with Figure 29. The horizontal circulation within the SVC for the Grow, Texas tornado is evident at the left in the time-lapse video from 8 to 15 seconds in (youtube.com/watch?v=XBNaq3B_t3M).

The first time-lapse takes place during the one to two minutes prior to the start of the tornado. At this time, an inflow channel was not observed around the low-level mesocyclone. The cloud base was relatively smooth and strong upward motion was not present around the base of the mesocyclone. The second time-lapse begins just prior to the tornado start time. Inflow, with a rapid upward motion, is observed wrapping around the low-level mesocyclone on the north and west side. Visually, the inflow channel connection is made near the tornado start time. As the tornado forms, downward motion is present just south of the tornado, where horizontal vortices are being created, and rapid cloud decay is occurring. Cloud erosion shows evidence of descending air (Markowski et al. 2003). Shortly after, on the northeast side of the tornado, a band of dust descends from near cloud level toward the ground in about 30 seconds. This is a great DRC observation, with the DRC descending from the nose of the dry slot, wrapping cyclonically around the RFD occlusion a few seconds before tornado formation. The DRC was detected by a horizontal vortex seen south of the tornado, and by dust seen descending from near cloud level towards the surface. As the tornado strengthens, the inflow channel, characterized with rapid vertical motion, is observed wrapping around the low-level mesocyclone. The SVC is observed northwest and north of the tornado, coincident with the inflow channel.

The environment in the Grow, Texas tornado case was very favorable for observation due to abundant dust. In spite that an SVC was documented, no SVC-supported circulations were observed. In Figure 29, the DRC, inflow channel and SVC are shown in a snapshot taken from the time-lapse sequence four minutes after the Grow, Texas tornado's start time at 6:38 pm CDT on May 4, 2022

While some model simulations suggest that the SVC is more vertically oriented (Orf et al. 2017), radar data and time-lapse videos suggest that the SVC in some storms orients around the mesocyclone in more of a horizontal manner. This could be because the RFD boundary pushes the SVC further north and west. In these cases, the storms are much more wrapped up and the SVC becomes an "updraft and downdraft process" that hugs the precipitation gradient of the hook. In other cases, the SVC could be oriented more vertically, but it would depend on environmental factors. The strongest horizontal vorticity generation within the SVC occurs along the forward flank, likely along the starting section of the inflow channel. If conditions are ideal, the horizontal tube of vorticity can remain intact as it goes around the western side of the mesocyclone.

Streamwise Vorticity Current (SVC), Inflow Channel (IC), Descending Reflectivity Core (DRC)

For Grow, Texas Tornado at 6:38 pm CDT on May 4, 2022 (Looking East)

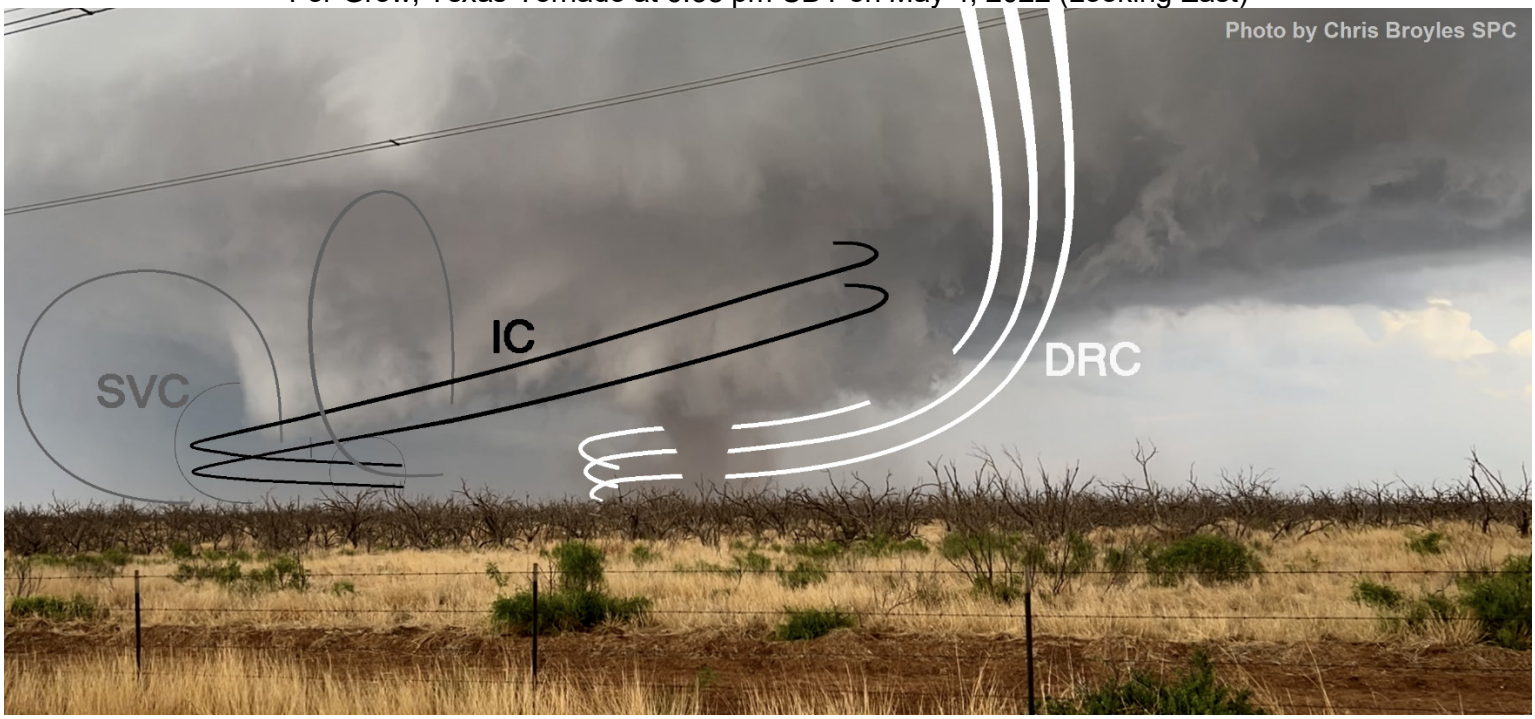

Figure 29. Time-lapse snapshot, 4 minutes after the start of the Grow, TX Tornado at 6:38 pm CDT on May 4, 2022. The photo looks east and shows the streamwise vorticity current (SVC), inflow channel (IC), and descending reflectivity core (DRC). In this case, the SVC appeared to be more horizontally oriented, which could be due to the RFD boundary pushing the SVC further north and west, to align with the forward flank precipitation gradient. Within a few minutes after this photo, the VROT reached 81 knots, signifying that it most likely produced winds capable of EF3 damage based on Smith et al. 2020 findings. Due to this, the storm qualifies as a high-end tornadic supercell, even though the tornado hit no structures and was officially rated EF Unknown.

The radar sequence for the Grow, Texas tornado on May 4, 2022 is shown in Figure 30. Using radar estimates, the circulation is between 7,450 and 7,800 feet in elevation. This is below the study's upper-end limit of 8,000 feet. While this case's relatively high elevation is a limitation, the radar still shows the features of tornadogenesis because supercells have key processes that form through a deep layer, sometimes deeper than what might be thought possible.

At 23 seconds prior to the tornado start time, a pronounced V-notch is evident. The RFD occlusion is located in the RFD's northeast quadrant and the RFD surge is ongoing (upper left panel). The DRC has already formed but the SVC has not yet developed. The RFD surge creates an inflow channel (upper right). At this time, the tornado has just started, with the nose of the DRC slightly to the north of the tornado. The new inflow channel coincides with SVC formation to the north and northwest of the tornado. The inflow channel and SVC lengthen as the tornado strengthens (lower left). The author's position is shown to the southwest of the SVC. This location is directly west of the tornado and west-northwest of the DRC. The SVC becomes fully developed (lower right), as the inflow channel wraps southward and southeastward towards the southern edge of the tornado. In elevation, the radar is likely sampling the very upper limit of the inflow channel.

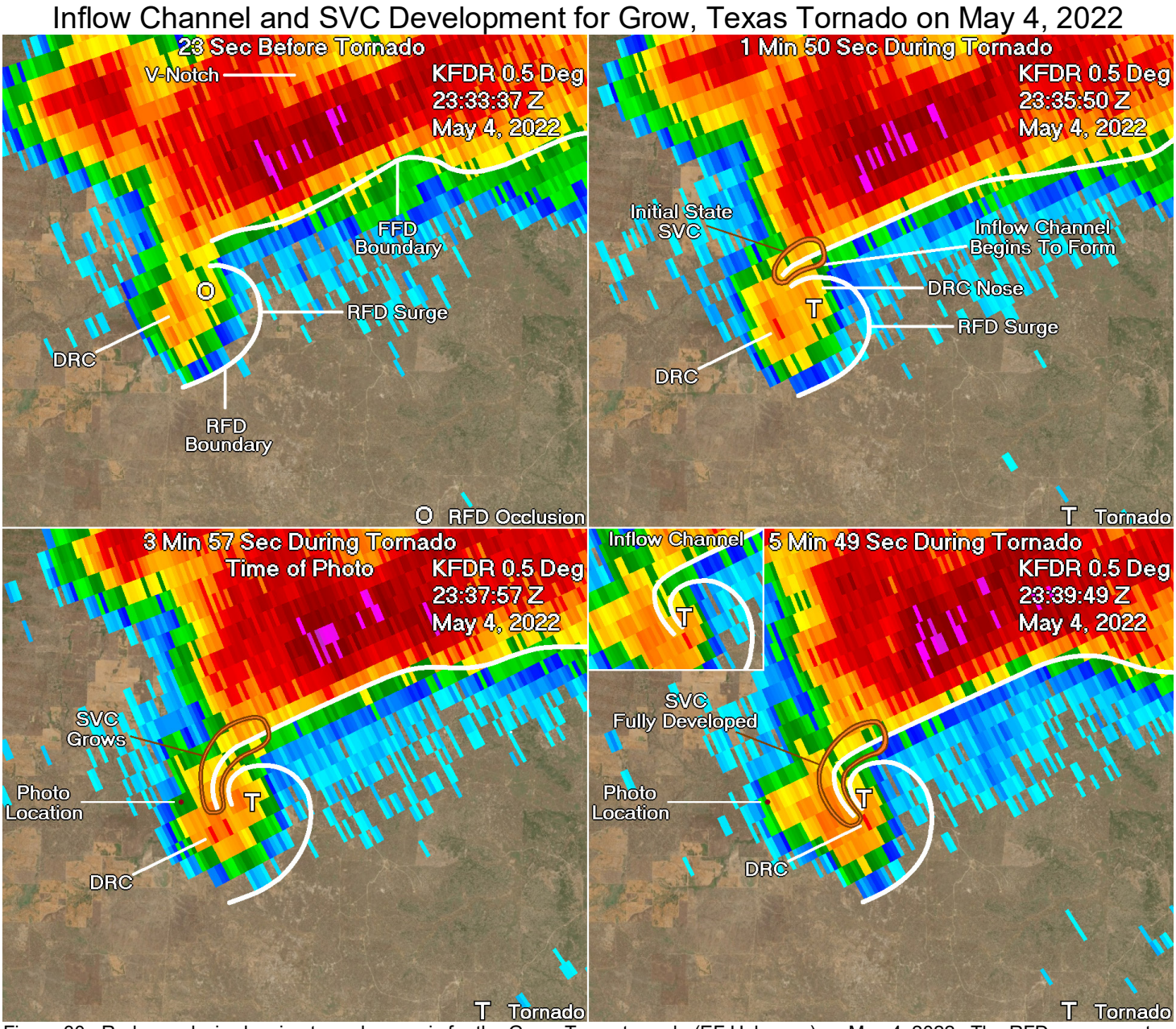

Figure 30. Radar analysis showing tornadogenesis for the Grow, Texas tornado (EF Unknown) on May 4, 2022. The RFD surge creates the inflow channel (upper two panels), which then coincides with SVC development. The tornado forms just south of the DRC's nose (upper right). As the inflow channel lengthens, the SVC grows and becomes fully developed (lower two panels).

8. TORNADOGENESIS TIMESCALE

In Figure 31, a hypothesized tornadogenesis timescale is shown. This graphic gives the average times of various events associated with tornadogenesis relative to the tornado start time based on the radar analysis in this study. Event times before the tornado start time are maroon, while those after the tornado start time are in blue. Sample sizes for each average time are in light gray.

For tornadogenesis according to this study, cell merger one starts the whole process around 15 minutes prior to the tornado start time, with the RFD surge beginning and the DRC initiating about a minute later. The RFD occlusion process begins approximately 10 minutes prior to the tornado and ends around 5 minutes before the tornado. Cell merger two strengthens the DRC at around 7 minutes before the tornado. The inflow channel and SVC form about 5 minutes before the tornado. The DRC arrives at the RFD occlusion near the start of the tornado. And the inflow connection is made about a minute after the tornado begins.

On this diagram, the average times were rounded to the nearest minute to avoid over-precision. Most of the scans used to do the analysis were spaced out in the 2 to 4 minute range. However, for some features, interpolation was done to

estimate times to about a minute and sometimes less. As the analysis ended and the last few cases were entered onto the spreadsheet, there were only small changes to the 208 case averages. For example, the last case entered for the Windsor, Colorado EF3 tornado on May 22, 2008, resulted in an average change of only 2 seconds for all key event times associated with tornadogenesis. Even though the times have been rounded to the nearest minute, the key timing of events is apparent. The events appear to work together, with each component contributing to tornadogenesis.

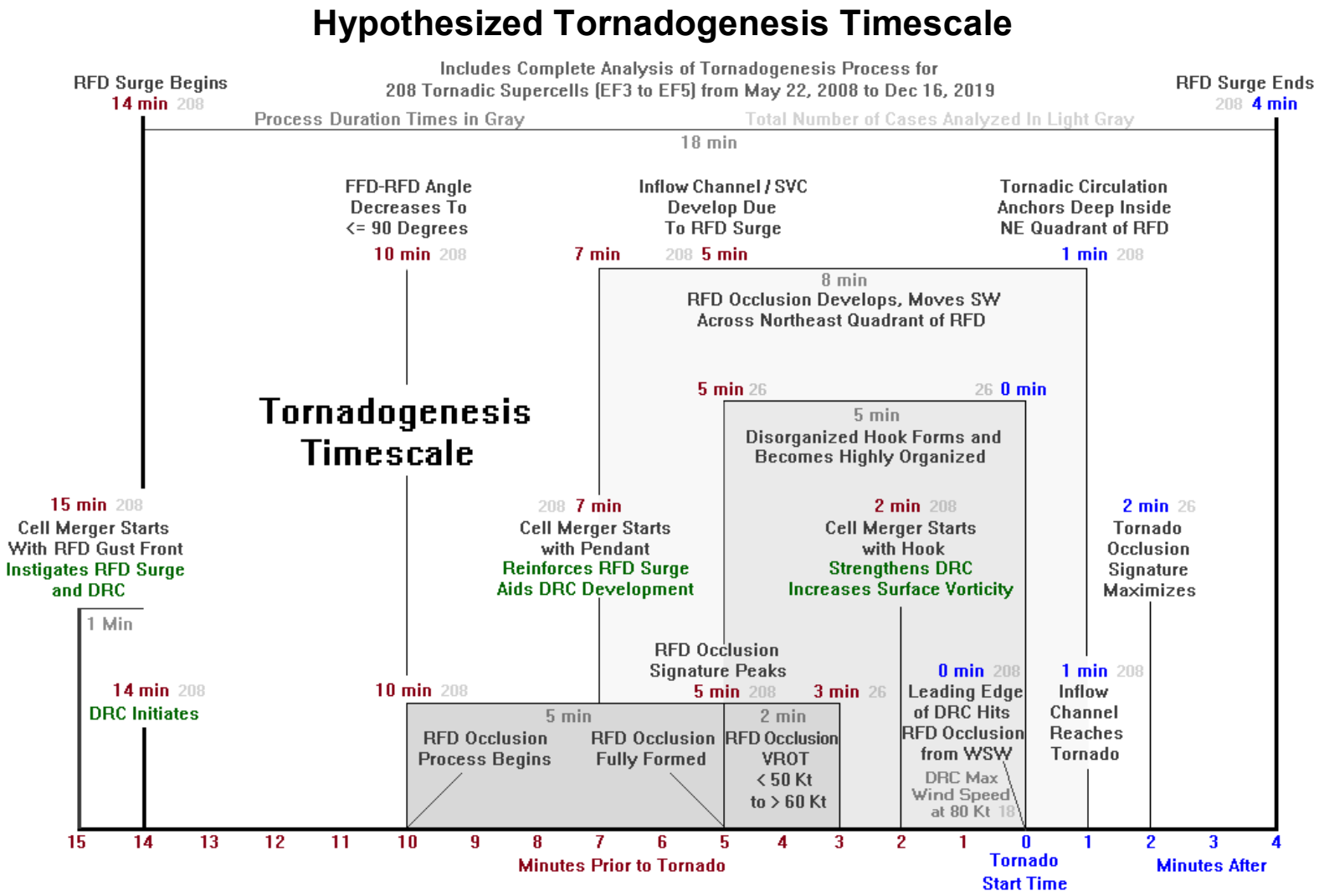

Figure 31. A timescale for high-end tornadic supercells using the 208 case averages, showing the events that occur during tornadogenesis. A cell merger starts the process around 15 minutes prior to the tornado by instigating the RFD surge and descending reflectivity core. The development of the RFD occlusion starts about 10 minutes before the tornado and matures about 5 minutes before the tornado. A second cell merger occurs about 7 minutes before the tornado. This reinforces the RFD surge and causes the DRC to strengthen. The DRC moves toward the RFD occlusion. The inflow channel and SVC start to develop at nearly 5 minutes before the tornado. A third cell merger occurs around 2 minutes before the tornado, which strengthens winds within the RFD occlusion and helps to increase vertical vorticity near the surface. The DRC arrives at the RFD occlusion, and the tornado forms nearly simultaneously. The tornado forms as the DRC wraps into the RFD occlusion. Finally, the inflow channel reaches the tornado about a minute after the tornado begins.

9. FINAL CONSIDERATIONS

Observations of a DRC, inflow channel and SVC were made on May 4, 2022 for the Grow, Texas tornado. Conditions where ideal for observing the wind motions around a supercell on that day, with abundant dust present between the surface and cloud level. This made it clear that no SVC-related circulations developed adjacent to the inflow channel.

Although, SVC-related circulations can occur, they appear to be rare. The two cases with an SVC circulation in this paper (Figure 26 and 28), both occurred as the tornado was ongoing and not before. The El Reno EF5 case in Figure 26, is the only example we found of an SVC-supported tornado merging with an RFD-related tornado. For that case, an important factor was the large cell merger that occurred with the forward flank of the El Reno EF5 supercell. It could be that the intense storm that moved into the El Reno supercell's inflow channel, tilted rotation along the forward flank to the surface, infusing high winds into the SVC-supported tornado.

In recent years, some new modeling studies of tornadic supercells place more emphasis on the inflow region of the supercell than the rear flank downdraft. In these simulations, the RFD appears to play an insignificant role. In these same simulations, there are often no cell mergers, no DRC and no inflow channel. It could be that the simulations are achieving tornadogenesis in ways that are different from the real world. Concerning these issues, the John Davies-Jones 2021 paper "Invented Forces in Supercell Models" is a good reference.

In some cases, the RFD surge is disregarded all together. In these simulations, the RFD surge is thought to be either the dry slot or a surge within the hook's precipitation to the west

of the tornado. There is no RFD surge to the east and north of the pre-tornadic circulation. In the real world, the RFD surge is usually a much larger feature, approaching the forward flank and pushing the inflow sector of the supercell back.

This study found that the RFD surge contributes to a rapid deepening of the RFD occlusion as the inflow channel and SVC are created. In addition, cell mergers and the DRC appeared to be important to tornado formation, helping a column of vertical vorticity to intensify. In this study, the RFD surge and DRC had a strong relationship to tornadogenesis.

Our suggestion to modelers is to begin thinking about ways to better model the RFD surge, DRCs and cell mergers. Modeling these features correctly can make the simulations more realistic and could tell us more about what is truly happening when supercells generate high-end tornadoes.

10. CONCLUSION

For this study, 208 supercells with EF3 to EF5 tornadoes were analyzed. For these events, it was found that the descending reflectivity core (DRC) was a common feature, appearing to have an important role in tornadogenesis. For the 208 case average, the DRC approached the RFD occlusion from the west-southwest at an average of near 50 knots, according to an estimate made using 20 cases. Based on radar analysis, the stronger downdraft winds inside the DRC hit the ground southwest of the RFD occlusion. For 18 cases within a quarter mile of the RFD occlusion, the DRC had an average wind speed maximum of over 80 knots. This area of high winds translates to the nose of the DRC as it approaches the RFD occlusion. When the nose of the DRC reaches the RFD occlusion, wind speeds dramatically increase within the column of vertical vorticity.

One hypothesis of this study is that the strong winds associated with the DRC cause some blocking of air to the southeast of the RFD occlusion. The winds trying to enter the RFD occlusion on the east side become more backed and speed up due to the Bernoulli Effect. The increase in wind speed coincides with reduced pressure within a cavity created by curvature just north of the DRC's nose. A theory suggests that this vertical column of vorticity rapidly strengthens within this curved cavity, aided by less vertical shear compared to that of the supercell's inflow sector. The protection offered by the DRC would enable the tornado to develop without being torn apart, making it easier for the low-level mesocyclone to stretch vertical vorticity upward. The 208 case average showed that the tornado forms as the leading edge of the DRC arrives at the RFD occlusion. Owing to the occurrence of these events, the DRC appears to play a major role in tornadogenesis. If rotation of the low-level mesocyclone is sufficiently strong when the DRC wraps into the center of the RFD occlusion, a high-end tornado will be possible.

The inflow channel and streamwise vorticity current (SVC) were also important features associated with high-end tornadic supercells examined here. According to this study, the inflow channel forms when the RFD surge takes place. The RFD surge pushes the RFD boundary north and east toward the FFD boundary. When the RFD boundary gets close enough to the forward flank, an inflow channel is created. This study estimated that winds that enter into the inflow channel approximately double. This was based on 14 cases that were high confidence within a sample of the 25 most recent cases in the database. This strong increase in wind speed in the inflow channel can be explained by the Bernoulli Effect, which also causes a sharp pressure drop in the inflow channel. The pressure is also hypothesized to drop across the northeast quadrant of the RFD as air is evacuated upward through the updraft at a faster rate than can be replaced below, due to restriction by the inflow channel. The pressure drop deepens a surface low in the RFD that likely increases rotation within the RFD occlusion.

Rapid vertical motion within the inflow channel, combined with the downdraft along the adjacent forward flank, cause the SVC to form. This study estimates that the SVC is located about 40 percent within the inflow channel and 60 percent within the forward flank downdraft. The SVC is estimated to be about 125 percent wider than the inflow channel, and forms adjacent to the inflow channel along its entire length.

The SVC was found in three states. The first state was the initial state, in which the SVC generation zone forms along the downdraft side of the inflow channel when moderate to heavy precipitation is present within the forward flank. The second state occurred when the SVC lengthened until it was impeded by the inflection point, where the RFD and FFD boundaries converge. At this stage, the inflection point likely cuts off the SVC. The third state occurred when the high-end tornado was ongoing, and the inflection point became washed out due to a high-level of supercell organization. At this time, the SVC would lengthen, taking a path southwest, south, and then southeastward along the eastern edge of the hook's precipitation gradient. Using this study's hypothesis for the location and timing of the SVC, a fully developed SVC was often observed when a high-end tornado was ongoing.

Three cases were examined in more detail for this study. The first case was the El Reno, Oklahoma EF5 tornado that occurred on May 24, 2011. The El Reno tornado developed at nearly the same time as an SVC-supported tornado. The SVC-supported tornado moved south and southeastward along the eastern edge of the hook's precipitation gradient, until reaching and merging with the RFD-related El Reno EF5 tornado.

The second case was the Bridge Creek, Oklahoma EF3 tornado that occurred on May 6, 2015. An SVC-supported circulation developed about 10 minutes after the Bridge Creek tornado formed. The SVC-supported circulation was estimated to be 600 to 800 feet in diameter, and just above the minimum detectable circulation size for high-resolution radar. The SVC-supported circulation moved south and southeastward down the eastern edge of the hook's precipitation gradient, similar to the El Reno case. Unlike the El Reno EF5 case, the vortex merger for the Bridge Creek EF3 case appeared to cause a rapid strengthening of the tornado.

The third case presented is the Grow, Texas tornado on May 4, 2022, that was estimated to have reached a wind speed of 120 to 165 mph based on VROT analysis (officially rated EF Unknown). The middle of this wind speed range is low-end EF3 meaning that it would be of similar strength to some of the EF3s in this dataset. The lead author took time-lapse of the tornadogenesis phase of this supercell. Two time-lapse sequences were taken. The first shows no evidence of the inflow channel one to two minutes prior to the tornado start time. The second time-lapse shows initial development of the tornado with an inflow channel wrapping around the low-level mesocyclone. The DRC could be seen interacting with the ground circulation near the tornado start time. Evidence of the DRC was documented on the south, east and north sides of forming tornado. The SVC was observed to the north of the inflow channel, straddling the inflow channel's northern edge and the forward flank downdraft. As the tornado developed, the SVC wrapped around the western side of the mesocyclone.

Radar analysis of the three cases substantiate this study's hypothesis that the SVC develops adjacent to the inflow channel, with the maximum horizontal vorticity generation occurring along the starting section of the inflow channel. And that the SVC extends southward and southeastward along the eastern edge of the hook's precipitation gradient when high-end tornadic supercells reach peak organization.

For questions about this study, please contact Chris Broyles at chris.broyles@noaa.gov.

11. ACKNOWLEDGEMENTS
We are extremely grateful to Israel Jirak for doing an excellent review of our papers. We are also thankful to the guidance that Patrick Skinner gave to us early on during our tornadogenesis project. Thanks also goes to John Hart and Brian Squitieri for giving guidance during the review process. Also, we are thankful to Paul Markowski and Jana Houser, who we consulted early in the project for guidance. Finally, we thank Ethan Broyles for giving us feedback concerning graphic presentation.

12. REFERENCES

Beck, J., and C. Weiss, 2013: An assessment of low-level baroclinity and vorticity within a simulated supercell. *Mon. Wea. Rev.*, **141**, 649–669.

Byko, Z. P. Markowski, Y. Richardson, J. Wurman, 2006: Radar reflectivity "blobs" observed by the Doppler on wheels. *Preprints, 23rd Conf. on Severe Local Storms*, St. Louis, MO, Amer. Meteor. Soc., 15.7.

Byko, Z., P. Markowski, Y. Richardson, J. Wurman, and E. Adlerman, 2009: Descending reflectivity cores in supercell thunderstorms observed by mobile radars and in a high-resolution numerical simulation. *Wea. Forecasting*, **24**, 155–186.

Davies-Jones, R. P., 2006: Tornadogenesis in supercell storms—What we know and what we don't know. Preprints, *Symposium on the Challenges of Severe Convective Storms,* Atlanta, GA, Amer. Meteor. Soc., P2.2.

Davies-Jones, R. P., R. J. Trapp, and H. B. Bluestein, 2001: Tornadoes and tornadic storms. *Severe Convective Storms,* C. A. Doswell, Ed., Amer. Meteor. Soc., 167–221.

Dixon, A, 2019: Emulated radar observations of near updraft vorticity in a simulated tornadic supercell. *Thesis*, University of Wisconsin-Madison.

Dixon, A., L. Orf, and K. Halbert, 2018: The streamwise vorticity current: Its origin and strategies for remote detection. *29th Conf. on Severe Local Storms*, Stowe, VT, Amer. Meteor. Soc., 84.

Dowell, D. C., and H. B. Bluestein, 1997: The Arcadia, Oklahoma, storm of 17 May 1981: Analysis of a supercell during tornadogenesis. *Mon. Wea. Rev.*, **125**, 2562–2582.

Fischer, J., J. M. L. Dahl, 2022: Supercell-External Storms and Boundaries acting as Catalysts for Tornadogenesis. Mon. Wea Rev., **150**.

French, M. M., P. S. Skinner, L. J. Wicker, and H. B. Bluestein, 2015: Documenting a rare tornado merger observed in the 24 May 2011 El Reno-Piedmont, Oklahoma supercell. *Mon. Wea. Rev.*, **143**.

Fujita, T., 1975: New evidence from April 3-4, 1974 Tornadoes: SMRP Research Paper No. 127.

Hane, C. E., and P. S. Ray, 1985: Pressure and buoyancy fields derived from Doppler radar data in a tornadic thunderstorm. *J Atmos. Sci.*, **42**, 18-35.

Houser, J. L., H. B. Bluestein, and J. C. Snyder, 2015: Rapid-scan, polarimetric, Doppler radar observations of tornadogenesis and tornado dissipation in a tornadic supercell: The "El Reno, Oklahoma" storm of 24 May 2011. *Mon. Wea. Rev.*, **143**, 2685–2710.

Houser, J., H. B. Bluestein, A. Seimon, J. Snyder, K. Thiem, 2018: Rapid-scan Mobile Radar Observations of Tornadogenesis. Amer. Geophy. Union, A54H-25.

Kennedy, A. D., J. M. Straka, and E. N. Rasmussen, 2007a: A statistical study of the association of DRCs with supercells and tornadoes. *Wea. Forecasting*, **22**, 1192–1199.

Kennedy, A. D., J. M. Straka, and E. N. Rasmussen, 2007b: A visual observation of the 6 June 2005 descending reflectivity core. *Electron. J. Severe Storms Meteor.*, **2**, 1–12.

Kennedy, A. D., J. M. Straka, and E. N. Rasmussen, 2006: The existence of descending reflectivity cores in rear flank appendages of supercells. Preprints, *23rd Conference on Severe Local Storms*, St. Louis, MO, Amer. Meteor. Soc., P10.4.

Klemp, J. B., and R. Rotunno, 1983: A study of the tornadic region within a supercell thunderstorm. *J. Atmos. Sci.*, **40**, 359–377.

Kosiba, K. A., J. Wurman, Y. Richardson, P. Markowski, P. Robinson, and J. Marquis, 2013: Genesis of the Goshen County, Wyoming, tornado on 5 June 2009 during VORTEX2. *Mon. Wea. Rev.*, **141**, 1157–1181.

Lee, B. D., C. A. Finley, and C. D. Karstens, 2012: The Bowdle, South Dakota, cyclic tornadic supercell of 22 May 2012: Surface analysis of rear-flank downdraft evolution and multiple internal surges. *Mon. Wea. Rev.*, **140,** 3419–3441.

Lee, B. D., C. A. Finley, and T. M. Samaras, 2011: Surface analysis near and within the Tipton, Kansas, tornado on 29 May 2008. *Mon. Wea. Rev.*, **139**, 370–386.

Lemon, L. R. and C. A. Doswell, 1979: Severe thunderstorm evolution and mesocyclone structure as related to tornadogenesis. *Mon. Wea. Rev.*, 107, 1184-1197.

Magsig, M. A., D. W. Burgess, D. C. Dowell, Y. Richardson, J. Wurman, 2002: The structure and evolution of hook echoes during tornadogenesis as revealed by high-resolution radar data. *21st Conference on Severe Local Storms*, San Antonio, TX, Amer. Meteor. Soc., pp. 473-476.

Markowski, P. A., 2002a: Hook echoes and rear-flank downdrafts: A review. Mon. Wea. Rev., **130**, 852-876.

Markowski, P. M., J. M. Straka, and E. N. Rasmussen, 2003b: Tornadogenesis resulting from the transport of circulation by a downdraft: Idealized numerical simulations. *J. Atmos. Sci.*, **60**, 795–823.

Markowski, P., and Y. Richardson, 2009: Tornadogenesis: Our current understanding, forecasting considerations, and questions to guide future research. *Atmos. Res.*, **93**, 3–10.

Marquis, J. N., Y. P. Richardson, J. M. Wurman, and P. M. Markowski, 2008: Single- and dual-Doppler analysis of a tornadic vortex and surrounding storm scale f low in the Crowell, Texas, supercell of 30 April 2000. Mon. Wea. Rev.,136, 5017–5043.

Murdzek, S. S., P. M. Markowski, and Y. P. Richardson, 2020: Simultaneous dual-Doppler and mobile mesonet observations of streamwise vorticity currents in three supercells. *Mon. Wea. Rev.*, **148**, 4859–4874.

Nowotarski, C. J., J. M. Peters, and J. P. Mulholland, 2020: Evaluating the effective inflow layer of simulated supercell updrafts. *Mon. Wea. Rev.*, **148**, 3507–3532.

Orf, L., R. Wilhelmson, A. Dixon, T. Halbert, 2018: The Role of the Streamwise Vorticity Current in Tornado Genesis and Maintenance. *Preprints, 29th Conf. on Severe Local Storms*, Stowe, VT, Amer. Meteor. Soc., 1.5.

Orf, L., R. Wilhelmson, B. Lee, C. Finley, and A. Houston, 2017: Evolution of a long-track violent tornado within a simulated supercell. *Bull. Amer. Meteor. Soc.*, **98**, 45–68.

Peters, J. M., C. J. Nowotarski, H. Morrison, 2019: What gives supercells the most intense updrafts of all modes of convection? *Amer. Geophy. Union*, A53U-3051.

Peters, J. M., C. J. Nowotarski, J. P. Mulholland, and R. L. Thompson, 2020: The influences of effective inflow layer streamwise vorticity and storm-relative flow on supercell updraft properties. *J. Atmos. Sci.*, **77**, 3033–3057.

Rasmussen, E. N., J. M. Straka, M. S. Gilmore, and R. P. Davies-Jones, 2006: A preliminary survey of rear-flank descending reflectivity cores in supercell storms. *Wea. Forecasting*, **21**, 923–938.

Satrio, M., 2022: A Triple-Doppler Analysis of the 17 May 2019 McCook / Farnam, NE tornadic supercell sampled during TORUS. Convective Seminar Spring 2022.

Schueth, A., 2018: Comparing observations and simulations of the streamwise vorticity current in a tornadic supercell storm, *Thesis*, Texas Tech University.

Schueth, A., C. Weiss, 2021: Comparing Observations and Simulations of the streamwise vorticity current and the forward-flank convergence boundary in a supercell storm. *Mon. Wea. Rev.*, **149,** 1651-1670.

Shabbott, C. J., and P. M. Markowski, 2004: Surface observations within forward-flank downdraft of a tornadic and nontornadic supercell. *Preprints, 22nd Conf. on Severe Local Storms*, Hyannis, MA, Amer. Meteor. Soc, P13.1.

Shabbott, C. J., and P. M. Markowski, 2006: Surface in situ observations within the outflow of forward-flank downdrafts of supercell thunderstorms. *Mon. Wea. Rev.*, **134**, 1422–1441.

Smith, B. T., R. L. Thompson, D. A. Speheger, A. R. Dean, C. D. Karstens, and A. K. Anderson-Frey, 2020a: WSR-88D tornado intensity estimates. Part I: Real-time probabilities of peak tornado wind speeds. *Wea. Forecasting*, **35**, 2479–2492.

Smith, B. T., R. L. Thompson, D. A. Speheger, A. R. Dean, C. D. Karstens, and A. K. Anderson-Frey, 2020b: WSR-88D tornado intensity estimates. Part II: Real-time applications to tornado warning time scales. *Wea. Forecasting*, **35**, 2493–2506.

Storm Data Publication, National Oceanic and Atmospheric Administration, National Centers for Environmental Prediction, https://www.ncdc.noaa.gov/stormevents/

Tanamachi, R. L., P. L. Heinselman, and L. J. Wicker, 2015: Impacts of a storm merger on the 24 May 2011 El Reno, Oklahoma, tornadic supercell. *Wea. Forecasting*, **30**, 501–524.

Wicker, L. J., 1996: The role of near surface wind shear on low-level mesocyclone generation and tornadoes. Preprints, *18th Conf. on Severe Local Storms,* San Francisco, CA, Amer. Meteor. Soc., 115–119.